INCREASING PROTON POLARIZATION IN AGS AND RHIC

Vahid H. Ranjbar

Submitted to the faculty of the Graduate School
in partial fulfillment of the requirements of the degree
Doctor of Philosophy in the Department of Physics
Indiana University

October 16, 2002

Accepted by the Graduate Faculty, Indiana University, in partial fulfillment of the requirements of the degree of Doctor of Philosophy.

_____

Shyh-Yuan Lee, Ph.D.

_____

Michael S. Berger, Ph.D.

Doctoral Committee

_____

John Carini, Ph.D.

October 16th, 2002

_____

John L. Challifour, Ph.D.

Acknowledgements

Many individuals have contributed much towards the production of this thesis. I am so lucky to have had the opportunity to work with so many outstanding experts in the field of accelerator physics. I feel especially lucky and thankful that Prof. S.Y.Lee took me on as his student and placed me at BNL. There I had the un-paralleled chance to work at the cutting edge of spin physics and make contact with many outstanding experts. I will be forever indebted to him for his valuable guidance and his constant concern for my success and well being.

I am also very grateful to Dr.W.MacKay my advisor at BNL for his constant support and time he devoted to assisting me in my many questions and problems. His door was always open to explain and discuss some of the finer aspects of accelerator physics. I would also like to thank Dr.T.Roser for his encouragement and judicious advise.

In addition I must thank Dr.M.Bai, Dr.V.Ptitsyn, Dr.A.Lehrach, Dr.A.Luccio, Dr.H.Huang and Dr.N.Tsoupas for all the help they provided to me at various times and the discussion, invaluable suggestions and insights into various problems in accelerator physics. I would also like to thank Dr.T.Satogata for always having time to solve my many computer related problems.

I would also like to acknowledge all the people who helped collect much of the invaluable data which made this thesis possible; J.W.Glenn, Dr.L.Ahrens, K.Brown and Dr.S.Tepikian.

I also wish to thank my committee members Dr.M.Berger and Dr.J.Carini for agreeing to take the time to be on my thesis committee and for allowing

me to take their courses in absentia. Of course I should not forget my physics hero Dr.J.Challifour for introducing me to the delights of Green functions and Mr.Shostakovich.

Finally I would like to thank my office mates R.Fliller and J.Cardona who kept me company in our little dungeon and off whom I always bounced ideas and discussed the many problems I had and who helped me solve more than a number of computer problems.

Abstract

Polarized protons were accelerated in AGS and RHIC up to 100 GeV during the 2002 polarized proton run. We examined some of the major sources of depolarization in both the AGS and RHIC. In the AGS uncorrected depolarization due to weak intrinsic resonances and coupled spin resonances result in a net loss on the order of 40%. We studied in detail the responses of these resonances to tune, skew quadrupole strength and partial snake strength and compared them against predictions given by an enhanced version of DEPOL [1].

Three solutions to the remaining weak and coupled spin resonances in the AGS were examined. An 11.4% partial solenoidal snake successfully flipped the spin during an intrinsic resonance crossing, the first time a strong partial snake has been tested in this way. Next we re-examine the proposal to add a family of 12 quadrupoles to the 15th lattice location in the AGS [2] to suppress the weak intrinsic resonances and proposed the addition of a second family of six skew quadrupoles in the 15th location to suppress the coupled spin resonances.

In RHIC higher order snake resonances were observed and measured for the first time. Their location and behavior appeared consistent with current snake resonance theory. Finally using the measured multipole fields along a fixed surface and current, a full field map was developed for RHIC's Siberian snakes. These field maps were used to help control and calibrate the orbit and spin tune in RHIC.

Contents

List of Tables

List of Figures

Chapter 1

Introduction

Spin is one of the more fascinating intrinsic properties of elementary particles. After being introduced by Uhlenbeck and Goudsmit in 1925 to explain the hyperfine splitting of the atomic spectra of hydrogen, its physical interpretation was not clearly understood until Dirac showed it as a natural consequence of relativity and quantum mechanics. As the boundaries of the Standard Model have been pushed, spin dependent interactions are now under increasing scrutiny. Since many of the properties of nucleons have been explained by properties of the constituent quarks, it was believed that the proton's spin could be explained by quark spin. However experiments at CERN and SLAC demonstrated that quarks carry only a portion of the total proton spin.

The question of the remaining spin is one of the problems the Relativistic Heavy Ion Collider (RHIC) spin program at Brookhaven National Labs seeks to understand. The approach is to examine the total and differential cross sections as result of elastic proton - proton scattering considering its dependency

on polarization at energies from 60 - 500 GeV. The W and Z bosons produced during the collisions are expected to violate parity maximally. From this parity violation the quark polarization in polarized protons can be measured by individual flavor. Thus using perturbative QCD the u and $\bar{d}$ polarization can be determined from W^+ production and the d and $\bar{u}$ polarizations from W^- production. In addition direct photon production from the collisions will allow the measurement of gluon polarization in the polarized proton.

These collisions also open the door for other searches for parity violations which go beyond the Standard Model. For example, a parity violation may occur in the interaction of quarks with substructure, or a new right-handed Z boson.

Thus a major concern in this effort is the delivery of polarized protons at these high energies. Since fields necessary to focus and accelerate the protons can also contribute to depolarization, a good understanding of the impact of various machine parameters is necessary if significant polarization is to be maintained.

In the absence of horizontal or longitudinal depolarizing fields all the spin vectors will precess around the vertical direction at a rate of $G\gamma$ per revolution in a circular accelerator. Here $G = \frac{g}{2} - 1$ is the anomalous magnetic moment coefficient and γ is the Lorentz factor. This rate of precession is known as the spin tune ν_s. The horizontal and longitudinal fields arising from dipoles, quadrupoles and solenoids can act in a coherent fashion to depolarize the beam. This can occur when the field perturbation tune equals the spin tune. These resonances phenomena can be broken down into three categories, imperfection resonances, intrinsic resonances and coupled spin resonances.

Imperfection resonances arise from the closed orbit in a realistic accelerator acquiring spin kicks from off-centered quadrupole fields. Thus, when the spin tune ν_s in an integer, the imperfection resonance condition is encountered. Intrinsic resonances are due to vertical betatron oscillations in the machine. In an accelerator with focusing and defocusing quadrupoles, particles with nonzero betatron oscillation amplitudes will traverse quadrupole fields off center and acquire spin kicks. When the spin tune ν_s equals a harmonic of the vertical betatron tune, an intrinsic resonance condition is encountered.

When a lattice contains skew quadrupoles, solenoids or rolls in the magnets the vertical and horizontal betatron motion can be coupled. In this case the frequency of the horizontal betatron motion is projected into the vertical plane. Thus the vertical motion acquires a second frequency component and a new resonance condition: coupled spin resonances. These resonances will occur when the spin tune ν_s equals a sideband of the horizontal betatron tune.

Thus, when accelerating polarized protons, a host of resonance conditions are encountered as $G\gamma$ increases. In the past, several techniques were devised to overcome these resonances. Initially imperfection resonances were overcome by using harmonic dipole correctors to correct the vertical closed orbit and a fast tune jump was used to avoid the intrinsic resonances. However both methods had significant short comings. The technique of harmonic correction proved very difficult since it was very sensitive to physical conditions inside the ring such as temperature and ground motion. Thus the process of correction was very tedious and time consuming. The fast tune jump method, since it is a non-adiabatic process can cause the undesirable emittance dilution of the beam.

Clearly as the energy level rises above 25 GeV to 100 and 250 GeV in RHIC, these methods simply become impractical. Luckily a clever solution to the problem of avoiding spin resonances was invented by Derbenev and Kondratenko [3]. They proposed placing in the lattice a powerful magnet to rotate the spin direction by 180° every time the beam circulated around the ring. Thus the precession rate of the proton's spin or spin tune ν_s is artificially made to be equal to 1/2. In this way all the resonance conditions are avoided and the spin tune is made energy independent. The type of magnet necessary to accomplish the full rotation of the spin vector is called a Siberian snake. The practical use of Siberian snakes was first demonstrated in 1989 at the Indiana University Cyclotron Facility (IUCF). [4] Later four super-conducting helical snakes were installed in RHIC (two per ring), and in 2001 and 2002 polarized protons were successfully accelerated to 100 GeV achieving 25% polarization [5] [6]. Despite the successful operation of the snakes in RHIC, several snake resonances were encountered during a number of the acceleration ramps. Snake resonances are new class of resonances which were first suggested to exist in accelerators with snakes by Lee and Tepekian in 1983 [7]. The theory of odd and even snake resonances was completed in 1992 by Lee [8]. Still with careful orbit correction and tune control these snake resonances can be avoided.

However in the AGS a full snake simply could not fit into the current lattice, so several other novel methods were pioneered in the AGS to overcome these resonances. In 1994 a partial snake was installed and tested in the AGS [13]. The partial snake was designed to rotate the spin vector by several degrees each turn. The result is the creation of a strong imperfection resonance at every $G\gamma = integer$. Since the resonance induced is strong enough to flip

the spin vector completely over, spin polarization can be preserved across the imperfection resonances. However since the partial snake was built using a solenoid, strong coupling was introduced into the AGS enhancing the coupled spin resonances.

In 1999 an ac dipole was installed and tested in the AGS [14]. The ac dipole was used to overcome strong intrinsic resonances by driving the ac dipole near the vertical betatron tune, thus enhancing the natural intrinsic resonance. So instead of depolarizing the beam a full spin flip is achieved. However, the ac dipole could not be used on the weak intrinsic resonances since the beam amplitude of the oscillation required to achieve a full spin flip in this case was beyond the physical aperture of the AGS beam pipe.

To date problems in the AGS remain with the weak intrinsic resonances and the coupled spin resonances. Problems with these resonances have hampered efforts to deliver the targeted 70% polarization levels in RHIC. The AGS has only been able to deliver a maximum of 40% polarization to RHIC, and during the latest 2002 polarized proton run only 25% was delivered due to the use of a backup main magnet power supply which provided a slower acceleration rate. The polarized proton source during the 2002 run reliably delivered protons polarized at 70% to the AGS. Thus losses in the AGS amount to nearly 40% of the delivered polarization, all of which are due to the coupled and weak intrinsic resonances. A better understanding of the behavior of these resonances is urgently needed so that an effective remedy can be implemented. While the snakes in RHIC seemed capable of preserving the delivered polarization up to 100 GeV, still snake resonances made the process erratic and unreliable. A proper understanding of the factors leading to depolarization is necessary so

that as RHIC is pushed to 250 GeV where even stronger resonances await, RHIC can reliably deliver polarized protons to the experiments.

This thesis begins with an overview of spin dynamics in Synchrotrons in chapter 2. Chapters 3-6 can be considered the first part dealing with AGS polarization issues. Chapters 7-8 can be considered the second part, dealing with RHIC polarization issues. In the first part I examined the problem of the remaining weak intrinsic and coupled spin resonances in the AGS. Here the development and testing of a new algorithm to calculate coupled spin resonances is presented and three possible solutions to these remaining resonances are discussed: the use of an additional family of quadrupoles to suppress the remaining weak intrinsic resonance, the use of an additional family of skew quadrupoles to suppress the coupled spin resonances and the use of a strong partial snake to cure both the imperfection and intrinsic resonances.

In the second part in Chapter 7, special attention is paid to the snake configuration in RHIC while in Chapter 8 evidence is presented for the very first observation of two higher order snake resonances in RHIC, the 1/4 even snake resonance and the 3/14 odd coupled snake resonance. in Chapter 9 we present our conclusions and suggestions for future issues which should be considered.

Chapter 2

General Theory of Spin Resonances in Synchrotrons

The dynamics of the spin vector of a charged particle is determined by the interaction of the magnetic moment with the surrounding magnetic field. In the particle's rest frame this is described simply by,

$$\frac{d\vec{S}}{dt} = \vec{\mu} \times \vec{B}. \tag{2.1}$$

Here $\vec{S}$ is the spin vector of a particle and $\vec{\mu}$ is the magnetic moment. If we transform to the laboratory frame then Eq. (2.1) becomes the Thomas-BMT (Bargmann, Michel, and Telegdi) Equation,

$$\frac{d\vec{S}}{dt} = \frac{e}{\gamma m}\vec{S} \times \left((1+G\gamma)\vec{B}_{\perp} + (1+G)\vec{B}_{\parallel} + (G\gamma + \frac{\gamma}{\gamma+1})\frac{\vec{E}\times\vec{\beta}}{c} \right). \tag{2.2}$$

$\vec{S}$ is the spin vector of a particle in the rest frame, and $\vec{B}_\perp$ and $\vec{B}_\parallel$ are defined in the laboratory rest frame with respect to the particle's velocity. $G = \frac{g-2}{2}$ is the anomalous magnetic moment coefficient, and γmc^2 is the energy of the particle. Neglecting the electric field, we can transform this equation by expanding about a reference orbit described by the Frenet-Serret coordinate system shown in Fig. 2.1. Thus we have

$$\frac{d\hat{x}}{ds} = \frac{\hat{s}}{\rho}, \quad \frac{d\hat{s}}{ds} = -\frac{\hat{x}}{\rho}, \quad \text{and} \quad \frac{d\hat{z}}{ds} = 0, \tag{2.3}$$

where ρ is the local radius of curvature for the reference orbit. Particle motion can be parameterized in this coordinate system as,

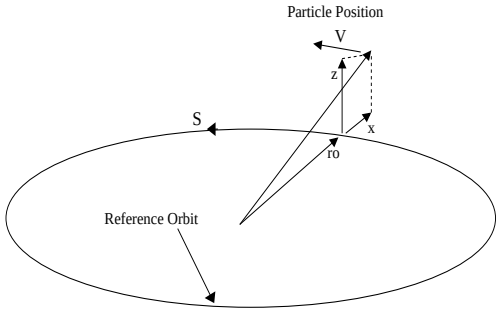

Figure 2.1: The curvilinear coordinate system for a particle motion in a circular accelerator. $\hat{x}$, $\hat{s}$ and $\hat{z}$ are the transverse radial, the longitudinal, and the transverse vertical unit base vectors, and $\vec{r}_0(s)$ is the reference orbit.

$$\vec{r} = \vec{r}_o(s) + x\hat{x} + z\hat{z}. \tag{2.4}$$

Here $\vec{r}_o(s)$ is the reference orbit and $\hat{s} = d\vec{r}_o/ds$. The velocity becomes

$$\vec{v} = \frac{d\vec{r}}{dt} = \frac{ds}{dt}\left(x'\hat{x} + \left(1 + \frac{x}{\rho}\right)\hat{s} + z'\hat{z}\right) \approx v(x'\hat{x} + \hat{s} + z'\hat{z}), \tag{2.5}$$

$$\vec{v}' = v\left(\left(x'' - \frac{1}{\rho}\right)\hat{x} + \frac{x'}{\rho}\hat{s} + z''\hat{z}\right). \tag{2.6}$$

All primes $'$ represent derivatives with respect to s. The transverse magnetic field can now be expressed as,

$$\vec{B}_\perp = \frac{1}{v^2}(\vec{v} \times \vec{B}) \times \vec{v} = B\rho\left(1 - \frac{x}{\rho}\right)\left[\left(x'' - \frac{1}{\rho}\right)\hat{z} + \frac{z'}{\rho}\hat{s} - z''\hat{x}\right]. \tag{2.7}$$

Where we have made use of $\frac{ds}{dt} \approx v(1 - x/\rho)$ and $\vec{v} \times \vec{B} = \frac{\gamma mc}{e}\frac{d\vec{v}}{dt}$. We should also note that $B_\perp\rho = \gamma mcv/e$ is the magnetic rigidity of the particle. To first order, $\vec{B}_\parallel$ can be found to be,

$$\vec{B}_\parallel \approx (B_s + B_z z')\hat{s}. \tag{2.8}$$

Using the dipole guiding field $B_z = -B_\perp\rho/\rho$, the B_s field can be derived from Maxwell's equations obtaining,

$$\frac{\partial B_s}{\partial z} = \frac{\partial B_z}{\partial s} = -\left(B\rho\right)\left(\frac{1}{\rho}\right)', \tag{2.9}$$

$$B_s = -B\rho z\left(\frac{1}{\rho}\right)'. \tag{2.10}$$

Neglecting higher order terms,

$$\vec{B}_{\|} \approx -B\rho \left(\frac{z}{\rho}\right)' \hat{s}. \tag{2.11}$$

Then using $\frac{d}{dt} = \frac{v}{\rho+x}\frac{d}{d\theta}$ the Thomas-BMT equation becomes

$$\frac{d\vec{S}}{d\theta} = \vec{S} \times \vec{F}, \tag{2.12}$$

where $\vec{F} = F_1\hat{x} + F_2\hat{s} + F_3\hat{z}$ and the elements are

$$\begin{aligned} F_1 &= -\rho z''(1+G\gamma) \\ F_2 &= (1+G\gamma)z' - \rho(1+G)\left(\frac{z}{\rho}\right)' \\ F_3 &= -(1+G\gamma) + (1+G\gamma)\rho x''. \end{aligned} \tag{2.13}$$

Using $\frac{d\hat{x}}{d\theta} = \hat{s}$, and $\frac{d\hat{s}}{d\theta} = -\hat{x}$ Eq. (2.12) becomes

$$\begin{aligned} \frac{dS_1}{d\theta} &= (1+F_3)S_2 - F_2S_3, \\ \frac{dS_2}{d\theta} &= -(1+F_3)S_1 + F_1S_3, \\ \frac{dS_3}{d\theta} &= F_2S_1 - F_1S_2. \end{aligned} \tag{2.14}$$

Expressed in the rotating frame Eq (2.12) then becomes

$$\frac{d\vec{S}}{d\theta} = \vec{n} \times \vec{S}. \tag{2.15}$$

Where $\vec{n} = -[F_1\hat{x} + F_2\hat{s} + (1 + F_3)\hat{z}]$. Since we are concerned only with spin 1/2 particles we can employ the well developed spinor formalism. Using the Pauli matrices

$$\sigma_x = \begin{pmatrix} 0 & 1 \\ 1 & 0 \end{pmatrix}, \sigma_s = \begin{pmatrix} 0 & -i \\ i & 0 \end{pmatrix}, \text{and } \sigma_z = \begin{pmatrix} 1 & 0 \\ 0 & -1 \end{pmatrix}, \tag{2.16}$$

the polarization can be given by

$$\vec{S} = \Psi^\dagger \vec{\sigma} \Psi. \tag{2.17}$$

Substituting Eq. (2.17) into the left side of Eq. (2.15) yields

$$\frac{d\vec{S}}{d\theta} = \frac{d\Psi^\dagger}{d\theta}\vec{\sigma}\Psi + \Psi^\dagger\vec{\sigma}\frac{d\Psi}{d\theta}. \tag{2.18}$$

Using $[\vec{\sigma}\cdot\vec{n}, \vec{\sigma}] = 2i(\vec{n}\times\sigma)$, the right hand side becomes

$$\vec{n}\times\vec{S} = -\frac{i}{2}(\Psi^\dagger\vec{\sigma})\vec{\sigma}\cdot\vec{n}\Psi + \frac{i}{2}\Psi^\dagger\vec{\sigma}\cdot n(\vec{\sigma}\Psi). \tag{2.19}$$

Finally equating both sides gives

$$\frac{d\Psi}{d\theta} = -\frac{i}{2}(\vec{\sigma}\cdot\vec{n})\Psi = -\frac{i}{2}\begin{pmatrix} G\gamma & -\xi \\ \xi^* & -G\gamma \end{pmatrix}\Psi. \tag{2.20}$$

Where $\xi(\theta) = F_1 - iF_2$ and to the first order we have neglected the $(1 + G\gamma)\rho x''$ term. Although the spinor wave function Ψ is similar in form to the quantum mechanical state function, in this case $\vec{S}$ is a classical vector. As in

the quantum mechanical case, however, this two component spinor is defined,

$$\Psi = \begin{pmatrix} u \\ d \end{pmatrix}. \tag{2.21}$$

Here u and d are complex numbers representing the up and down components. The components of the spin vector become

$$\begin{aligned} S_1 &= u^* d + u d^* \\ S_2 &= -i(u^* d - u d^*) \\ S_3 &= |u|^2 - |d|^2. \end{aligned} \tag{2.22}$$

Because $H = (\vec{\sigma} \cdot \vec{n})$ is hermitian,

$$|\vec{S}| = |u|^2 + |d|^2 = \Psi^\dagger \Psi \tag{2.23}$$

and the magnitude of the spin vector remains constant. The normalization condition for the spinor wave function is chosen to be $\Psi^\dagger \Psi = 1$.

When $H = (\vec{\sigma} \cdot \vec{n})$ is independent of θ the spinor wave function can be propagated using,

$$\Psi(\theta_2) = e^{-\frac{i}{2} H(\theta_2 - \theta_1)} \Psi(\theta_1). \tag{2.24}$$

In the case where there are no longitudinal and radial fields ($\xi = 0$) the spinor wave function becomes simply

$$\Psi(\theta_2) = e^{-i\frac{G\gamma}{2}(\theta_2 - \theta_1)\sigma_z} \Psi(\theta_1). \tag{2.25}$$

Thus we see that the spinor wave function will precess at a rate of $G\gamma$ turns per revolution around the ring. This rate of precession is known as the spin tune. Eq. (2.24) can be re-expressed using the spin transfer matrix formalism so that $e^{-\frac{i}{2}H(\theta_2-\theta_1)} = t(\theta_2, \theta_1)$. The spin transfer matrix in the case of a one turn map becomes

$$t(\theta_i + 2\pi, \theta_i) = e^{-i\pi\nu_s \hat{n}_{co}\vec{\sigma}} \tag{2.26}$$

where ν_s is the spin tune and $\hat{n}_{co}$ is the spin closed orbit. The spin closed orbit represents the unit vector around which the spin will precess as it orbits the ring.

Depolarization of the spinor state function occurs when transverse or longitudinal fields perturb the spin at the rate equal to the same fractional frequency of the spin tune. These spin resonances can be broken down into three basic types; imperfection, intrinsic and coupled spin resonances. All three are a result of spin kicks accumulated from vertical beam motion through quadrupoles. They differ in the causes of the vertical motion. Imperfection resonances arise from vertical closed orbit errors which are due to errors in the alignment and field of the magnetic elements which comprise the lattice of the accelerator. Since these errors are typically uncorrelated random errors they perturb the spin once every period around the lattice and thus become significant when the spin tune crosses an integer ($G\gamma = integer$). Intrinsic resonances are due to the natural vertical betatron oscillations as the particle traverses the lattice. This vertical oscillation rate is known as the vertical betatron tune ν_z. Spin kicks due to vertical betatron oscillations can add coherently when the fractional part of the spin tune equals the vertical betatron tune. Coupled spin

Imperfection	$G\gamma = \mathrm{N}$
Intrinsic	$G\gamma = \mathrm{N} \pm \nu_z$
Coupled	$G\gamma = \mathrm{N} \pm \nu_x$

Table 2.1: Three classes of spin resonances. N = *integer*.

resonances can occur in the presence of coupling elements such as solenoids and skew quadrupoles. When linear coupling is present, the vertical oscillations around the ring will acquire an additional frequency component from the horizontal betatron tune ν_x.

These three resonance conditions can be summarized in Table 2.1. These resonances are particularly strong when N is a multiple of the periodicity of the lattice.

To assess the magnitude of the resulting depolarization, the depolarizing elements in Eq. (2.20) can be expanded in a Fourier series yielding,

$$\xi(\theta) = F_1 - iF_2 = \sum_K \varepsilon_K e^{-iK\theta} \tag{2.27}$$

where the Fourier coefficient or resonance strength ε_K is given by,

$$\varepsilon_K = -\frac{1}{2\pi} \oint \left[(1+G\gamma)(\rho z'' + iz') - i\rho(1+G)(\frac{z}{\rho})' \right] e^{iK\theta} d\theta \tag{2.28}$$

and K is the resonance spin tune.

The effect of crossing an isolated resonance under a constant acceleration rate permits an analytical solution to Eq. (2.20) yielding an expression for the

final polarization known as the Froissart-Stora formula [9],

$$< S_z >= 2e^{-\pi \frac{|\varepsilon|^2}{2\alpha}} - 1, \tag{2.29}$$

where $\alpha = \frac{dG\gamma}{d\theta}$ is the acceleration rate.

2.1 Snakes and Snake Resonances

A clever technique to avoid spin depolarizing resonances was proposed by Derbenev and Kondratenko [3], using a local spin rotator to achieve a 180° rotation of the spin vector about an axis in the horizontal plane. These spin rotators are known as Siberian snakes. They force the spin tune in an accelerator to be 1/2 and thus energy independent. In this way all the imperfection, intrinsic or coupled spin resonance conditions can be avoided.

However the work of Lee and Tepikian showed that when the normal resonance strength is large a new class of spin-depolarizing resonance conditions can occur [7] . These resonances are due to coherent higher-order spin-perturbing kicks and are located at

$$\nu_s + lK = integer, \qquad (l = integer). \tag{2.30}$$

Here ν_s is the spin tune, K is the spin-depolarizing resonant harmonic and l indicates the order of the snake resonance. Since the location of intrinsic resonant condition depends on the vertical betatron tune, the snake resonance

condition is equivalent to

$$\delta\nu_z = \frac{\nu_s \pm k}{l}, \tag{2.31}$$

where $\delta\nu_z$ is the fractional part of the betatron tune and k is any integer.

These snake resonances can be further classified in terms of l = odd or even. Odd snake resonances are due to the coherent enhancement of the intrinsic resonance by the spin perturbing kicks of the snake. Thus their strength depends primarily on the strength of the associated intrinsic or coupled spin resonance and the acceleration rate. However $l = even$ snake resonances do not manifest themselves until machine errors are introduced. In 1992 Lee showed that the introduction of errors in the machine would cause these even order snake resonances to appear [8]. The introduction of closed orbit errors result in imperfection resonances which with the snake, overlap the nearby intrinsic resonance. The result of these overlapping resonances is the generation of even order snake resonances. The existence of an imperfection resonance can perturb the spin tune by

$$\nu_{s,\max/\min} = \frac{1}{2} \pm \frac{1}{\pi} \arcsin[\sin^2 \frac{\pi\varepsilon_{imp}}{N_s}] \tag{2.32}$$

during the crossing of an imperfection resonance. Due to the spin tune perturbation shown in Eq. (2.32), each snake resonance will spit into two separated by

$$\delta\nu_z \leq |\frac{1}{\pi l} \arcsin[\sin^2 \frac{\pi\varepsilon_{imp}}{N_s}]| \tag{2.33}$$

The strength of the imperfection serves to enhance the strength of the snake resonances and split these resonances by a width given by Eq. (2.33).

Chapter 3

Techniques for Calculation of the Resonance Strength

Currently DEPOL is the primary software used to calculate spin resonance strengths due to imperfection and intrinsic resonances. The algorithm used is based on Courant's and Ruth's paper [1] where the integral in Eq. (2.28) is evaluated by breaking it up into a sum over each element in the lattice:

$$\varepsilon_K = \sum_{lattice} \varepsilon_{K_m}, \tag{3.1}$$

where

$$\varepsilon_{K_m} = -\frac{1}{2\pi}\int_{s_1}^{s_2} \{(1+K)(z'' + \frac{iz'}{\rho}) - i(1+G)(\frac{z}{\rho})'\} e^{iK\theta(s)} ds. \tag{3.2}$$

Assuming that $1/\rho$ is a step function, constant in the element and zero just outside the element, partial integration leads to an intermediate form,

$$\varepsilon_{K_m} = \frac{1}{2\pi}\left[\frac{(1+K)(\xi_1+i)}{\rho} z_1 e^{iK\theta_1} + \frac{(1+K)(\xi_2-i)}{\rho} z_2 e^{iK\theta_2} \right. \\ \left. -(1+K)\int_{s_1}^{s_2} z'' e^{iK\theta} ds - \frac{K}{\rho^2}(K-G)\int_{s_1}^{s_2} z e^{iK\theta} ds\right], \qquad (3.3)$$

where ξ_i are contributions due to edge focusing of the magnet and $z_i = z(s_i)$. Applying partial integration again we obtain,

$$\varepsilon_{K_m} = \frac{1}{2\pi}\left[\frac{(1+K)(\xi_1+i)}{\rho} z_1 e^{iK\theta_1} + \frac{(1+K)(\xi_2-i)}{\rho} z_2 e^{iK\theta_2} - (1+K)\times \right. \\ \left. \left((z_2' - \frac{iK}{\rho} z_2) e^{iK\theta_2} - (z_1' - \frac{iK}{\rho} z_1) e^{iK\theta_1}\right) + (\frac{K(K^2+G)}{\rho^2}) \int_{s_1}^{s_2} z e^{iK\theta} ds\right]. \qquad (3.4)$$

In the uncoupled case this integral is evaluated using the homogeneous equation $z'' = -k_z z$. Substitution using this equation allows an exact evaluation of Eq. (3.4).

In the case of linear coupling however, the homogeneous equation is no longer valid for all the elements. So we proceed by block diagonalizing the individual transfer matrices for the coupling elements. Thus we hope to transform the z coordinate into a basis where a new homogeneous equation is true. The technology to accomplish this has been already developed by Teng [10]. Given an element with off diagonal values in the 4×4 transfer matrix,

$$\mathbf{M}_e = \begin{pmatrix} A_e & B_e \\ C_e & D_e \end{pmatrix}, \qquad (3.5)$$

the 2×2 submatrices A,B,C and D can be used to develop a transformation which will block diagonalize M_e. (The subscripts e denote that only single element transfer matrices are being considered as opposed to the one turn transfer matrix.) The result is

$$\mathbf{R}_e \mathbf{M}_e \mathbf{R}_e^{-1} = \begin{pmatrix} E_e & 0 \\ 0 & F_e, \end{pmatrix} \tag{3.6}$$

$$R_e = \frac{1}{\sqrt{1+|r_e|}} \begin{pmatrix} I & -\overline{r_e} \\ r_e & I \end{pmatrix}, \tag{3.7}$$

$$\overline{r}_e = -\left(\frac{Tr(A-D)}{2} \pm \sqrt{|B+\overline{C}| + \frac{Tr^2(A-D)}{4}} \right) \frac{B+\overline{C}}{|B+\overline{C}|}. \tag{3.8}$$

The bar on C indicates a symplectic conjugate, which is defined as

$$\overline{C} = -SC^T S, \tag{3.9}$$

with S being the matrix

$$S = \begin{pmatrix} 0 & 1 & & & & \\ -1 & 0 & & & & \\ & & 0 & 1 & & \\ & & -1 & 0 & & \\ & & & & . & \\ & & & & & . \end{pmatrix}. \tag{3.10}$$

Working with the canonical pairs $(x, p_x/p_s)$ and $(z, p_z/p_s)$ with $p_z/p_s \approx z'$ and

$p_x/p_s \approx x'$ outside each element, we can use R_e to transform them to a locally uncoupled basis a, a', b, b' using,

$$\begin{pmatrix} x \\ x' \\ z \\ z' \end{pmatrix} = R_e^{-1} \begin{pmatrix} a \\ a' \\ b \\ b' \end{pmatrix}. \tag{3.11}$$

In this basis the homogeneous equations $a'' = -k_a a$ and $b'' = -k_b b$ will hold. $k_a$and k_b can be determined by considering that most elements can have their transfer matrices cast in the form [1],

$$\begin{pmatrix} a_2 \\ a_2' \end{pmatrix} = \begin{pmatrix} \cos(\varphi_a) & \frac{\sin(\varphi_a)}{\sqrt{k_a}} \\ -\sqrt{k_a}\sin(\varphi_a) & \cos(\varphi_a) \end{pmatrix} \begin{pmatrix} a_1 \\ a_1' \end{pmatrix}. \tag{3.12}$$

Thus $k_a = -\frac{E_{e_{2,1}}}{E_{e_{1,2}}}$and $k_b = -\frac{F_{e_{2,1}}}{F_{e_{1,2}}}$. So to solve the integral in Eq. (3.4) we can write $z = [r_{e_{1,1}} a + r_{e_{1,2}} a' + b]\frac{1}{\sqrt{1+|r_e|}}$ to obtain,

$$\int_{s_1}^{s_2} z e^{ik\theta} ds = -\frac{1}{\sqrt{1+|r_e|}} \int_{s_1}^{s_2} \left[r_{e_{1,1}} \frac{a''}{k_a} + \frac{b''}{k_b} - r_{e_{1,2}} a' \right] e^{iK\theta} ds. \tag{3.13}$$

Now using an integration technique similar to the original DEPOL [1] paper,

$$\int_{s_1}^{s_2} a'' e^{iK\theta} ds = \frac{(a_2' - \frac{iK}{\rho} a_2) e^{iK\theta_2} - (a_1' - \frac{iK}{\rho} a_1) e^{iK\theta_1}}{1 - K^2/k_a\rho^2}, \tag{3.14}$$

[1]Here k_a and k_b may be complex.

we obtain a final closed expression,

$$\int_{s_1}^{s_2} ze^{iK\theta}ds = \frac{1}{\sqrt{1+|r_e|}} \left[\left(\frac{iK}{\rho}r_{e_{1,2}} - r_{e_{1,1}}\right)\left(\frac{(a_2' - \frac{iK}{\rho}a_2)e^{iK\theta_2} - (a_1' - \frac{iK}{\rho}a_1)e^{iK\theta_1}}{k_a - K^2/\rho^2}\right)\right.$$
$$\left. - \left(\frac{(b_2' - \frac{iK}{\rho}b_2)e^{iK\theta_2} - (b_1' - \frac{iK}{\rho}b_1)e^{iK\theta_1}}{k_b - K^2/\rho^2}\right) + r_{e_{1,2}}(a_2e^{iK\theta_2} - a_1e^{iK\theta_1})\right]. \quad (3.15)$$

Thus our final expression for the resonance contribution from each element is,

$$\varepsilon_{K_m} = \frac{1}{2\pi}\left[\frac{(1+K)(\xi_1+i)}{\rho}z_1e^{iK\theta_1} + \frac{(1+K)(\xi_2-i)}{\rho}z_2e^{iK\theta_2}\right.$$
$$- (1+K)\left((z_2^{'} - \frac{iK}{\rho}z_2)e^{iK\theta_2} - (z_1^{'} - \frac{iK}{\rho}z_1)e^{iK\theta_1}\right) + \left(\frac{K(K^2+G)}{\rho^2}\right)$$
$$\times\left[\frac{1}{\sqrt{1+|r_e|}}\left((\frac{iK}{\rho}r_{e_{1,2}} - r_{e_{1,1}})\left(\frac{(a_2' - \frac{iK}{\rho}a_2)e^{iK\theta_2} - (a_1' - \frac{iK}{\rho}a_1)e^{iK\theta_1}}{k_a - K^2/\rho^2}\right)\right.\right.$$
$$\left.\left. - \left(\frac{(b_2' - \frac{iK}{\rho}b_2)e^{iK\theta_2} - (b_1' - \frac{iK}{\rho}b_1)e^{iK\theta_1}}{k_b - K^2/\rho^2}\right) + r_{e_{1,2}}(a_2e^{iK\theta_2} - a_1e^{iK\theta_1})\right)\right]\Bigg]. \quad (3.16)$$

Of course for those elements which are already block diagonal we can neglect the local rotation to a diagonal basis and employ the original form,

$$\int_{s_1}^{s_2} ze^{iK\theta}ds = \frac{(z_2' - \frac{iK}{\rho}z_2)e^{iK\theta_2} - (z_1' - \frac{iK}{\rho}z_1)e^{iK\theta_1}}{k_z - K^2/\rho^2}. \quad (3.17)$$

3.1 Implementation of the New DEPOL Algorithm

DEPOL derives the $z_{1,2}$ and $z'_{1,2}$ values necessary to evaluate the resonance amplitude from MAD software [11]. However when MAD evaluates under conditions of linear coupling it employs u and v coordinates which correspond to the bloc diagonal basis for the one turn transfer matrix. To correctly evaluate the resonance strength we must transform back to the original basis to obtain x, x', z, z'. So in our code we read in values for the R matrix and use it to transform the u, u', v, v' back to the x, x', z, z' basis. From here we can then implement Eq. (3.16) or (3.17) for each element.

There is an additional complication in the implementation of this program which is an expression of the subtleties of Eq. (2.28). In the original DEPOL code implicit use was made of the properties of the enhancement function $\zeta_N(x)$ [22] which is defined as

$$\zeta_P(x) = \frac{\sin P\pi x}{\sin \pi x}. \tag{3.18}$$

For $x = N$ ($N = 0, \pm 1, \pm 2, ...$), $\zeta_P(x)$ goes to $(-1)^N P$ for even P and P for odd P. When $G\gamma$ is on a resonance, the enhancement function yields the exact contribution to the resonance amplitude from one turn around all the elements in the accelerator lattice. However since we are dealing with a Fourier expansion in non-integer K values, the actual integral in Eq. (2.28) must go from minus infinity to plus infinity. When evaluating resonances due to linear coupling an integral only once around the lattice will yield a superposition

of enhancement functions due to both vertical and horizontal tunes. In this case we are forced to integrate Eq. (2.28) over many passes to obtain a good approximation for the resonance strength. This slows the functioning of the code down considerably.

However if we look closely at the behavior of the elements which make up the integral to be evaluated in Eq. (2.28), it appears that we can factor out the phase element which changes with each period around the lattice. The remaining elements in the sum remain constant for each pass. The factored phase elements can be evaluated analytically using the properties of a geometric series. The result is four separate enhancement functions,

$$\begin{aligned} E_u(N)_\pm &= \sum_{n=0}^{N} e^{i2\pi n(K\pm\nu_u)} \\ &= \pm e^{iN\pi(K\pm\nu_u)} \frac{\sin\left(\pi(N+1)(K\pm\nu_u)\right)}{\sin\left(\pi(K\pm\nu_u)\right)} \\ E_v(N)_\pm &= \sum_{n=0}^{N} e^{i2\pi n(K\pm\nu_v)} \\ &= \pm e^{iN\pi(K\pm\nu_v)} \frac{\sin\left(\pi(N+1)(K\pm\nu_v)\right)}{\sin\left(\pi(K\pm\nu_v)\right)} \end{aligned} \tag{3.19}$$

Here ν_u and ν_v the betatron tunes in the uncoupled u and v basis. N the number of passes around the lattice. The function once evaluated can then be multiplied by the appropriate terms in the sum over one pass in the lattice (see Appendix B for details).

Another issue concerns the measurement of emittance. Normally most operations software is set up to evaluate the emittance provided there is no coupling. So a method was developed to transform incorrect measurements

taken in the AGS for the emittance, ϵ_x and ϵ_y values and transform them to correct measurements of ϵ_u and ϵ_v. This is detailed in appendix C.

Chapter 4

The Configuration of the AGS

The Brookhaven Alternating Gradient Synchrotron (AGS) is the third stage in a complex of accelerators which accelerates polarized protons to 25 GeV. The fourth and final stage culminates in the Relativistic Heavy Ion Collider (RHIC) which takes protons and gold ions up to 250 GeV and 100 GeV respectively. For polarized protons the process begins with a source of optically pumped polarized ions of H^- (OPPIS) [12]. These ions are then accelerated to 200 MeV through a radio frequency quadrupole in a linear accelerator. They are then strip-injected into the AGS booster and accelerated to 1.5 GeV. During injection in the AGS only one bunch of the 12 rf buckets were filled and accelerated to 25 GeV for final injection into RHIC. The full scheme is shown in Fig. 4.1

In the AGS a partial solenoidal snake was employed to overcome imperfection resonances [13], and an ac dipole was used to overcome strong intrinsic resonances [14]. In past years the AGS was operated with an acceleration

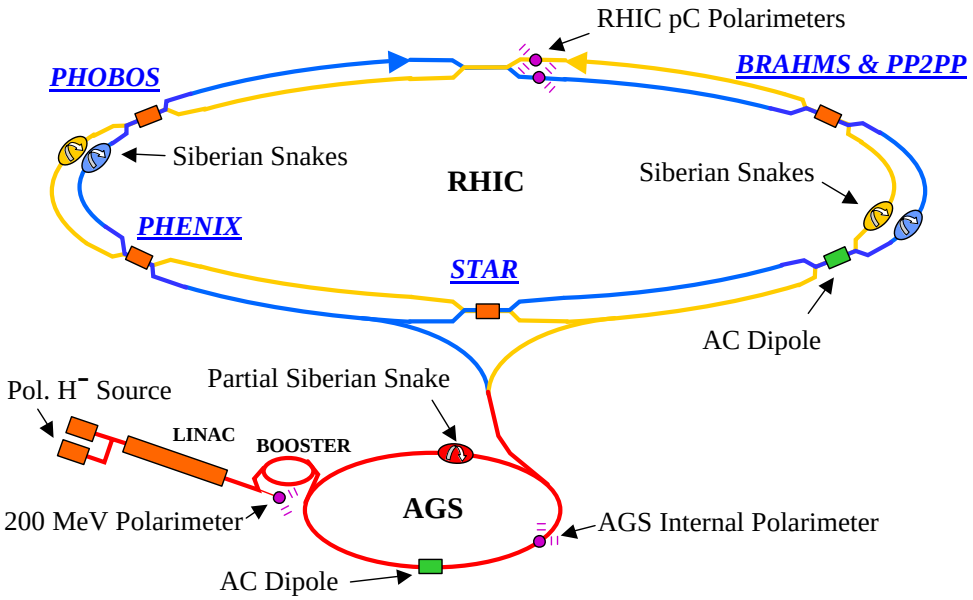

Figure 4.1: Schematic of the AGS and RHIC complex.

rate of $\frac{dG\gamma}{d\theta} = \alpha = 4.8 \times 10^{-5}$, where G is the anomalous magnetic moment coefficient and θ the orbital bending angle. However during the 2002 run a backup power supply was used for the magnets resulting in a ramp rate of $\alpha = 2.4 \times 10^{-5}$. The lower acceleration rate made the use of a weaker partial snake possible since at a slower acceleration rate effective spin flipping due to the imperfection resonances is enhanced. Lowering the partial snake strength has the advantage of reducing the effective strength of the coupled spin resonances but this is offset by an increase in the depolarization during weak intrinsic resonance crossing (a direct consequence of the Froissart-Stora formula) . In the past a 5% partial snake was used. During this run a modified partial snake ramp was found to be the most effective. The current control

of the partial snake was set up to start with a 3% snake from injection at $G\gamma = 7.5$ and ramp up to 5% by $G\gamma = 21$.

The AGS is also equipped with a family of six skew quadrupoles located in the 17th straight section of superperiods B,D,F,H,J and L next to the horizontal tune quadrupoles. They are 0.39088 m in length and the current can range from 0 to a maximum of 500 A which corresponds to $\int \frac{\partial B_z}{\partial z} ds = 0.84$ T. In addition a family of 12 vertical and horizontal tune quadrupoles are located in the 3rd and 17th straight section of each superperiod. They have the same length and current to field transfer ratio as the skew quadrupoles.

4.1 Polarization Measurement

At 200 MeV the beam polarization is measured with elastic scattering from a carbon fiber target. In the AGS polarization was measured using the internal polarimeter installed in the 20th straight section of the C super-period designed for energies of 4 GeV to 25 GeV. The polarimeter measured left-right asymmetry of the $p-p$ elastic scattering processes of a proton beam scattering off a Carbon target. The polarimeter consists of two recoil arms oriented at 77.25° away from the beam on the left and right side. These arms each held two scintillator counters, a hodoscope, Al wedge, dE/dX counter and a Veto counter. In this way the left-right asymmetry was measured and calculated:

$$\delta = \frac{\sqrt{L\uparrow R\downarrow} - \sqrt{L\downarrow R\uparrow}}{\sqrt{L\uparrow R\downarrow} + \sqrt{L\downarrow R\uparrow}}. \tag{4.1}$$

Here $L\uparrow$ and $L\downarrow$ are the number of events in the left arm when the beam polarization is up and down respectively, and $R\uparrow$ and $R\downarrow$ are the number of events in the right arm. To reduce systematic error the polarization alters direction between up and down for every AGS cycle. From the left-right asymmetry measurement δ, beam polarization P can be calculated,

$$P = \frac{1}{A}\delta. \tag{4.2}$$

The analyzing power A was determined using an empirical formula from [15].

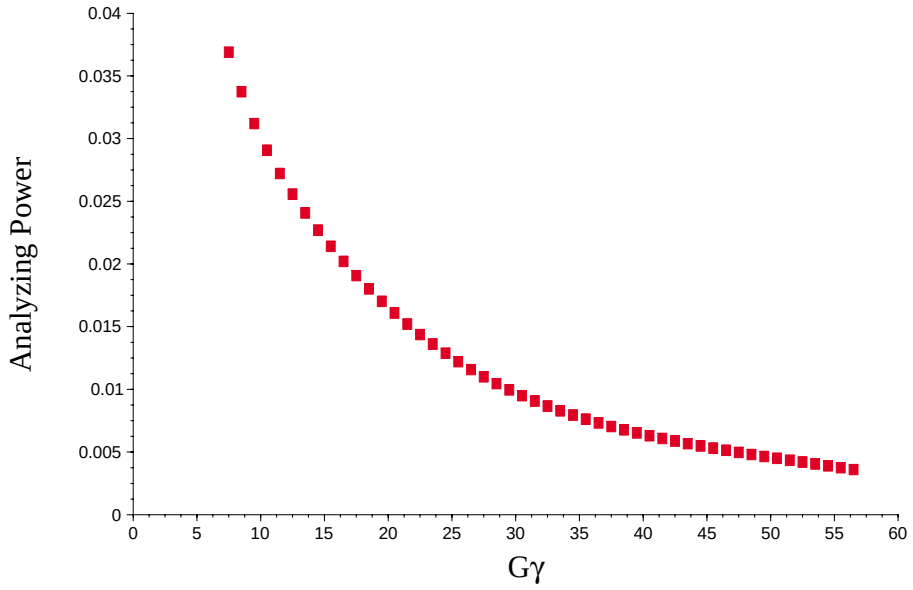

Figure 4.2: Analyzing power A as a function of $G\gamma$. Data obtained from [16].

4.2 AGS Partial Snake

The partial solenoidal snake is located in the 10th straight section of the I super-period. It is 2.43 meters long with a maximum integrated strength of 4.7 T-m [17]. A 100% snake achieves a full 180° spin rotation, while a 5% snake can only achieve 5% of 180° or a $\phi = 9°$ spin rotation. In the presence of this perturbation the spin tune ν_s will deviate from $G\gamma$ according to

$$\cos \pi\nu_s = \cos \pi G\gamma \cos \frac{\phi}{2}. \tag{4.3}$$

With $\phi = 9°$ the spin tune will never equal an integer, and thus the imperfection resonance condition is avoided completely. For a given solenoidal field strength the corresponding spin rotation angle ϕ drops off with momentum. Thus the solenoid must be ramped along with acceleration in order to maintain a constant spin rotation angle ϕ.

4.3 AGS ac Dipole

The ac dipole was first installed and tested in the AGS in 1999 [14]. It is located in the 10th straight section of superperiod A. It is 0.8128 m long by 0.3048 m wide by 0.2225 m high.The whole assembly forms a resonant LC circuit. The ac dipole was driven by an amplified WavTek function generator. At each of the strong intrinsic resonances $0 + \nu_z$, $12 + \nu_z$ and $36 \pm \nu_z$ the generator was triggered by the AGS Gauss Clock system.

One of the major concerns during operation of the ac dipole is to control

the separation between the ac dipole's drive frequency and the vertical betatron tune. If the frequency separation is too large then a full spin flip is unachievable, but if the frequency is too close then the beam can be lost or have too much emittance growth. During the 2002 polarized proton run this proved to be a significant problem due to current fluctuations in the AGS tune quadrupoles. Of particular concern was the $0 + \nu_z$ resonance crossing which required a coherence resulting in the loss of a portion of the beam on the aperture. As well, the benefit of the ac dipole during the $36 + \nu_z$ resonance crossing came into question so the use of the ac dipole during the $36 + \nu_z$ resonance crossing was abandonedin the final days of the 2002 run.

Chapter 5

Comparision with Experimental Results

During the 2002 polarized proton run we had the opportunity to gather data on the response of the weak intrinsic and coupled spin resonances in the AGS to various tune settings, solenoidal strength settings and skew quadrupole settings. What follows is a presentation of this data compared with calculated results using the enhanced version of DEPOL in conjunction with MAD. Fitting our experimental data to MAD and DEPOL calculations required the consideration of rolls in the main combined function magnets. These rolls account for the observed skew quadrupole moment observed in the 'bare' AGS (ie. with only the main combined function magnets on). Figs. 5.1 - 5.2 show the results of scan in energy versus polarization from $G\gamma = 7.5$ to 46.5. Along with this we plotted the corresponding DEPOL calculated polarization values for the corresponding acceleration and emittance values. These scans where

taken by adjusting the AGS main magnet function to ramp up to six successively higher flattop values from $G\gamma = 7.5$ to 46.5.

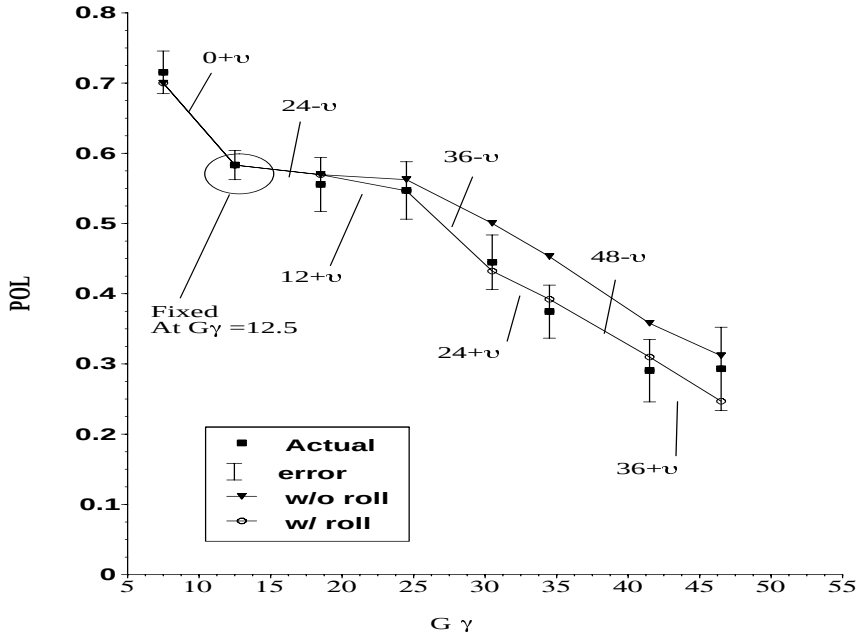

Figure 5.1: Polarization versus $G\gamma$ scan taken in a 6 hour period during the 2002 polarized proton run in the AGS. Due to miscalibration of the ac dipole at $0 + \nu_z$ we fixed the $G\gamma = 12.5$ to the measured value. By including rolls in the main bending magnets coupling is enhanced thus fitting more accurately our measured data.

For this case the baseline DEPOL calculation was fixed to the $G\gamma = 12.5$ asymmetry measurement of 14.9×10^{-3} with 25.55×10^{-3} analyzing power (polarization = 58.3%). This was done because crossing the $0 + \nu_z$ resonance using the ac dipole proved to be problematic during this particular run. To

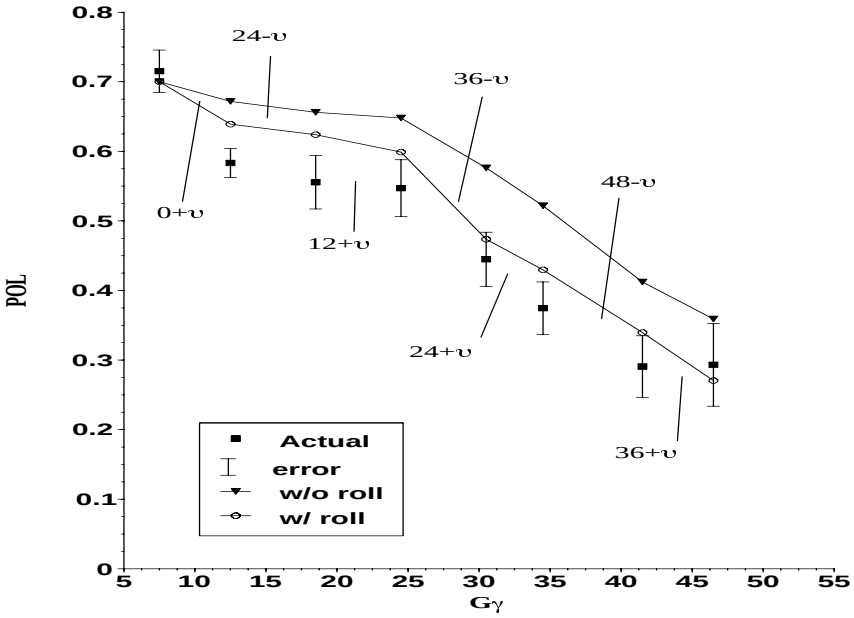

Figure 5.2: Polarization versus $G\gamma$ scan taken in a 6 hour period during the 2002 polarized proton run in the AGS. This is the same plot as Fig. 5.1 with out fixing $G\gamma = 12.5$ to the measured value.

obtain a maximum polarization transmission the necessary coherence ends up scrapping a portion of beam on the beam pipe aperture. The effects of this are not clearly understood. In my opinion the sensitivity of this crossing has been the dominating factor in determining the variability of our asymmetry measurements which at top energy ($G\gamma = 46.5$) ranged from 0 to 1.8×10^{-3}. However we found that 1.5×10^{-3} was a very reproducible value. Additionally at $G\gamma = 12.5$ it was possible to produce a maximum asymmetry of 16.4×10^{-3} if properly tuned.

5.1 Study of Weak Instrinsic Resonances

At several of the flattop settings we found time to perform a quick scan of the response of polarization to tune for the weak intrinsic resonances. These graphs are shown in Figs. 5.4 to 5.6. Since we did not have the use of a horizontal tune meter throughout the whole 2002 run, all DEPOL calculations were made using the measured input currents to the horizontal and vertical tune quadrupoles. The tunes quoted in all the AGS graphs are set point tunes. Since much work in the past has been devoted to developing an accurate model of the AGS lattice for use in MAD, tune calculation performed in the MAD model present a good representation of the actual tunes in the AGS. In Fig. 5.3 the bare AGS and MAD tune calculations are shown to be in good agreement.

In Fig. 5.4 we can see a plot of polarization at $G\gamma = 18.5$ versus the horizontal tune at the $24-\nu$ resonance crossing. We found that attempts to correct the 9th orbital harmonic while on the $G\gamma = 18.5$ flattop ramp produced a large polarization response. These corrections caused a variation in asymmetry from 10×10^{-3} to 9×10^{-3}. The sensitivity of asymmetry measurements to orbit corrections support speculation that this extra loss is due to the feed down from the sextupole fields. So we see that the addition of closed orbit errors can effect the strength and structure of intrinsic resonances. Another possible explanation is the existence of uncorrected imperfection resonances. In fact there is a precedence for this supposition, since earlier on during this experiment the existence of a corrected imperfection resonance between $G\gamma = 30.5$ and $G\gamma = 34.5$ prompted a modification of the partial snake strength and the construction of a modified snake ramping routine. In this routine the

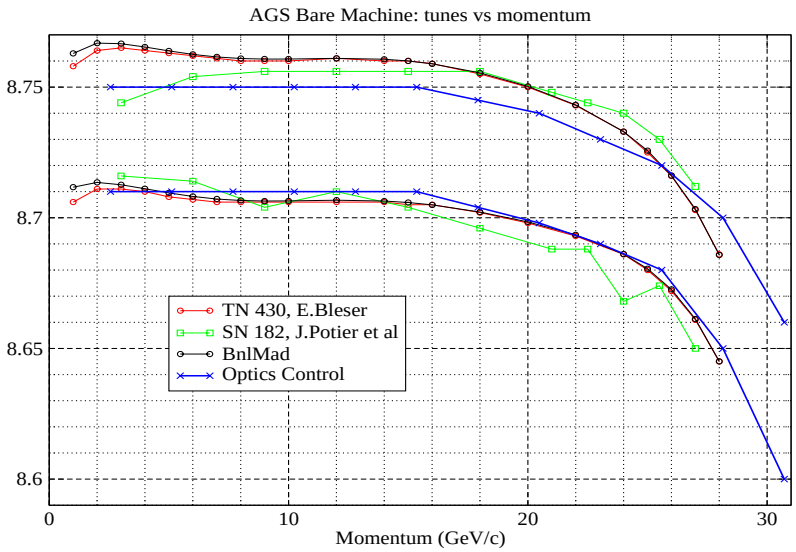

Figure 5.3: AGS bare machine tunes are plotted versus momentum. Here line labeled SN 182 represent the measured tunes performed by J. Poiter, et. al., the line labeled TN43 and Bnlmad represent MAD calculations from two lattices and the line labeled optics control represents the current tune control program's predictions.[18]

snake was kept at 3% from injection to $G\gamma = 12 + \nu$ and ramped up to 5% to $G\gamma = 46.5$. Possibly a combination of effects could explain the deviation from the expected DEPOL values, since vertical closed orbit errors could introduce both uncorrected imperfection resonances and an intrinsic resonance effect through the feed down of sextupole fields in the vertical plane.

In Figs. 5.5 to 5.6 we see further evidence which the role an uncorrected closed orbit could be playing. Across all of these resonances it was found that the introduction of a vertical closed orbit error $z_{rms} > 1$ mm could improve

the fit of DEPOL calculations through the sextupole feed down. The best estimate of closed orbit errors in the AGS range from $z_{rms} = 1$ to 2 mm . In future runs, much consideration should be given to correct the orbit since an uncorrected orbit can both hamper the performance of the partial snake and modify the structure of the intrinsic resonances.

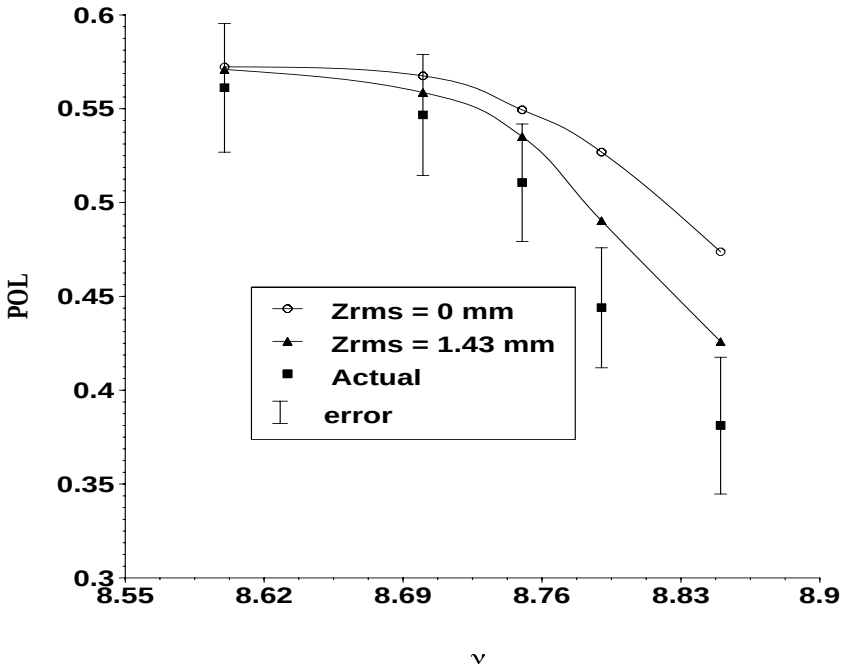

Figure 5.4: $24-\nu$ resonance crossing as a function of horizontal tune measured at $G\gamma = 18.5$ flattop plotted with DEPOL predictions assuming initial polarization was the same as measured at $G\gamma = 12.5$, 58%. Plots are with and without added closed orbit distortions $Z_{\rm rms} = 1.43$mm and $X_{\rm rms} = 0.067$mm. Emittances in vertical were 10π mm-mrad.

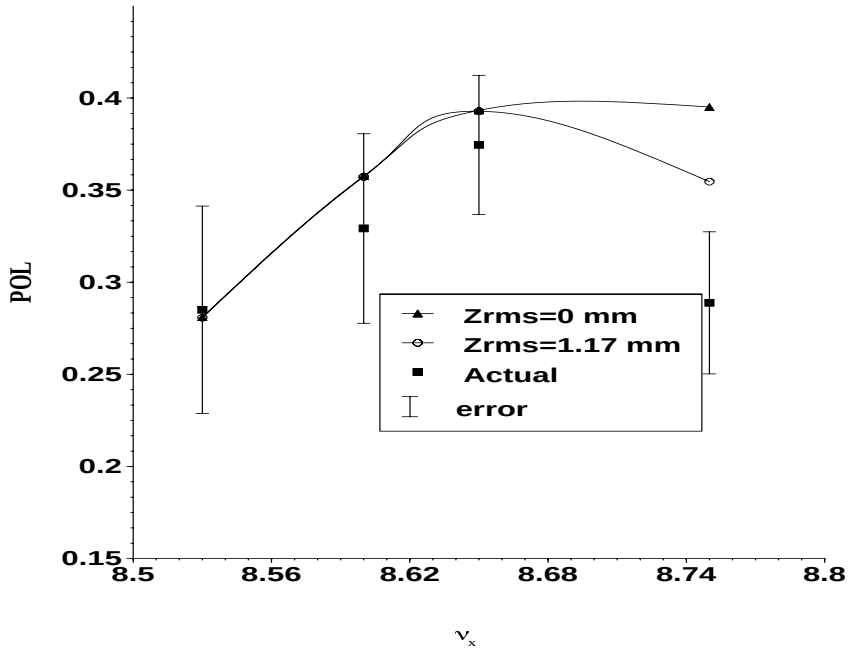

Figure 5.5: $24+\nu$ resonance crossing as a function of horizontal tune measured at $G\gamma = 34.5$ flattop plotted with DEPOL predictions assuming initial polarization at $G\gamma = 30.5$ to be 43%. Plots with and without added closed orbit distortions $Z_{\rm rms} = 1.17$mm and $X_{\rm rms} = 0.079$mm. Emittances in the vertical were 23π mm-mrad.

5.2 Study of Coupled Spin Resonances

The primary source of coupling in the AGS is the partial solenoidal snake. In addition there exists a family of six skew quadrupoles. It has been observed that the bare AGS machine has a net skew quadrupole moment. Work with slow beam extraction has also shown that a family of skew quadrupoles needs to be powered at 50 A in order to alleviate the effects of coupling in the bare AGS. Using this value an estimate of the magnitude of the average roll was found to be 0.15 mrad. Coupling studies from 15 years ago estimated the

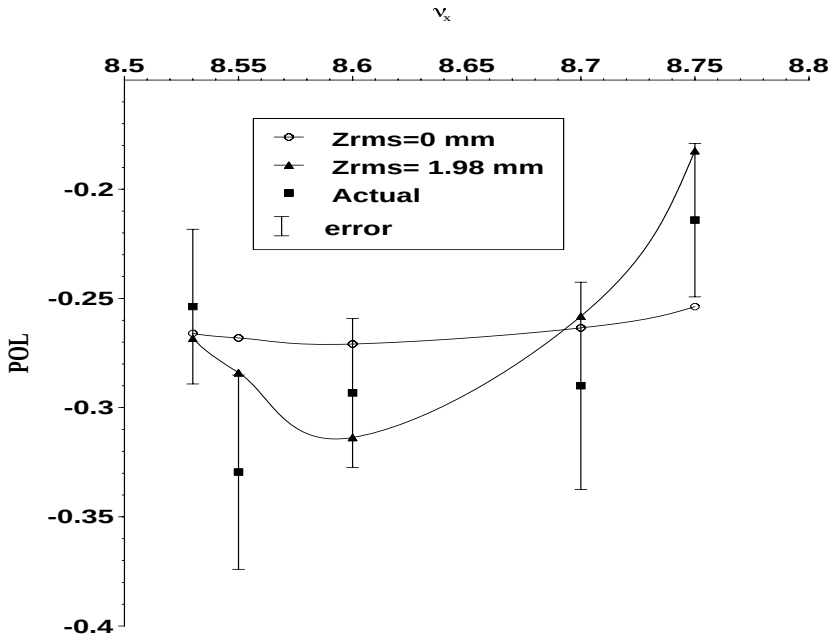

Figure 5.6: $48 - \nu$ resonance crossing as a function of horizontal tune measured at $G\gamma = 41.5$ flattop, plotted with DEPOL predictions assuming initial polarization at $G\gamma = 34.5$ to be 32%. Curves are with and without added closed orbit distortions $Z_{\rm rms} = 1.98$mm and $X_{\rm rms} = 0.13$mm. Emittances in the vertical were 23π mm-mrad.

average roll to be 0.13 mrad [19].

Additionally closed orbit errors can contribute to coupling via feed down from the sextupole fields present in the AGS combined function magnets and sextupole magnets. However for the coupled spin resonance calculations closed orbit errors did not seem to have as profound an effect on the structure of the response of the resonance as it did for the weak intrinsic calculations. The inclusion of closed orbit errors served only to shift the whole curve without affecting the overall structure.

During the 2002 polarized proton run, particular attention was paid to studying the impact of the coupled spin resonances during the $0+\nu$ resonance crossing. This was done because at this low energy the analyzing power of the AGS polarimeter was sufficiently large to generate accurate measurements and the strength of the $0+\nu$ coupled spin resonance was large. Initial DEPOL calculations without rolls generated curves which were too broad. It was only by including either a large single roll or selectively placed rolls that a good fit to the measured data was achieved. For all DEPOL calculations shown here I have included selectively distributed rolls applied to the CF magnets [1] (0.05 mrad per magnet) and applied to the BD magnet [2] (0.25 mrad per magnet). This is not unreasonable considering previous estimates. However it should be emphasized that this configuration is by no means unique. While it was essential to include a net skew quadrupole moment in the bare AGS, the distribution and the direction of these rolls is still unclear since many different configurations could fit our data. Either a survey of these rolls needs to be commissioned or perhaps a method similar to the "action phase jump technique" [20] used in RHIC could be used in the AGS.

In Figs. 5.7 - 5.9 one can see the results of our tune scans, snake scans and skew quadrupole scans. All calculations assume a 70% polarization at injection into the AGS. In all cases we were able to achieve a good agreement between simulated and measured polarization.

[1] CF is the label for a family of combined function focusing magnets located at 13,14,17 and 18 positions in each super-period

[2] BD s the label for a family of combined function defocusing magnets located at 11,12,19 and 20 positions in each super-period

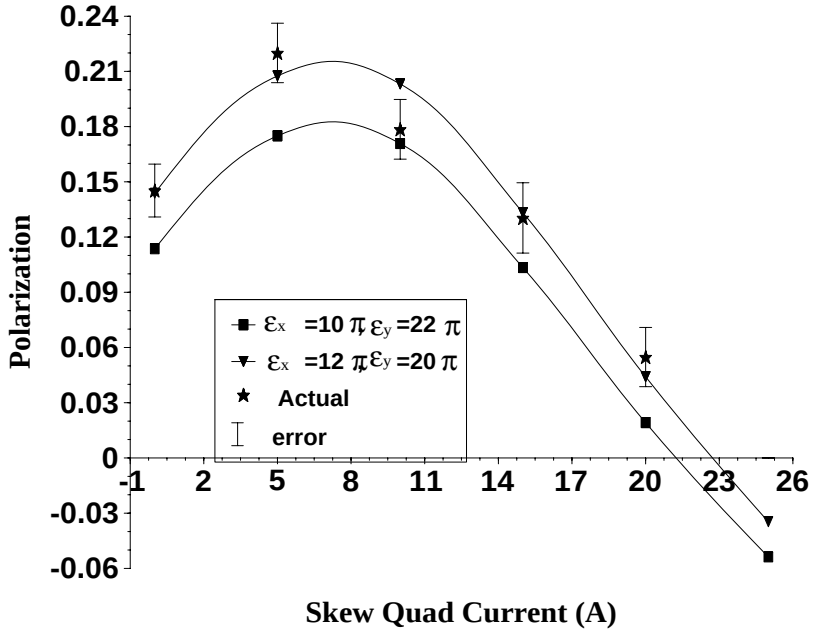

Figure 5.7: Polarization after crossing the $0+\nu_x$ and $0+\nu_z$ resonances with fixed vertical and horizontal tunes ($\nu_z = 8.8$, $\nu_x = 8.78$). Scanning through skew quadrupole input currents from 0 to 25 Amps. The vertical and horizontal emittances were measured at $(11 \pm 1)\pi$ and $(21 \pm 1)\pi$ mm-mrad. In addition a distributed roll was applied to the BD and CF magnets as described in this section.

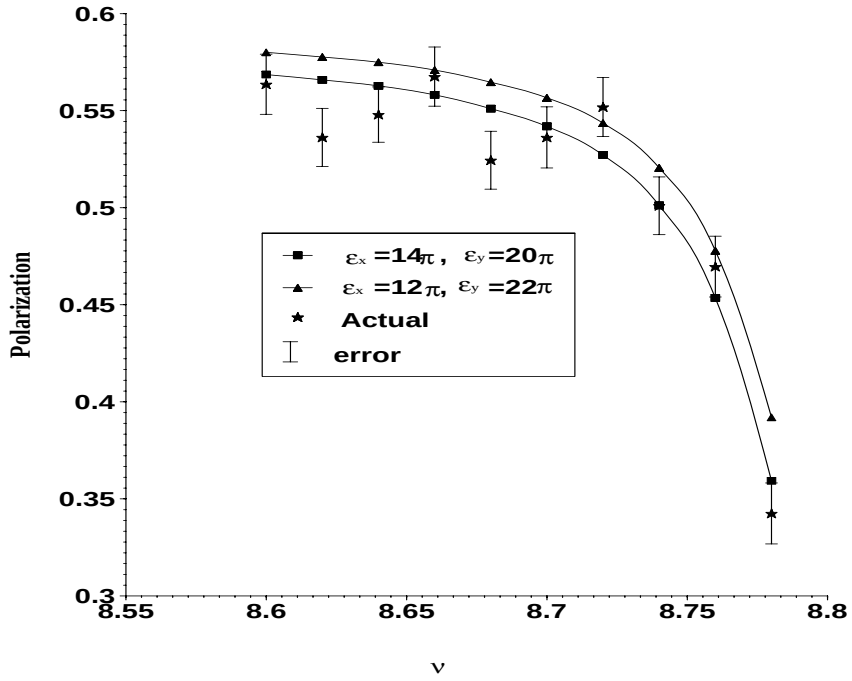

Figure 5.8: Polarization after crossing the $0+\nu_x$ and $0+\nu_z$ resonances with fixed vertical tune ($\nu_z = 8.8$) scanning horizontal tunes. Vertical and horizontal emittances were measured at $(13 \pm 1)\pi$ and $(21 \pm 1)\pi$ mm-mmrad respectively for DEPOL calculations. In addition a distributed roll was applied to the BD and CF magnets as described in this section.

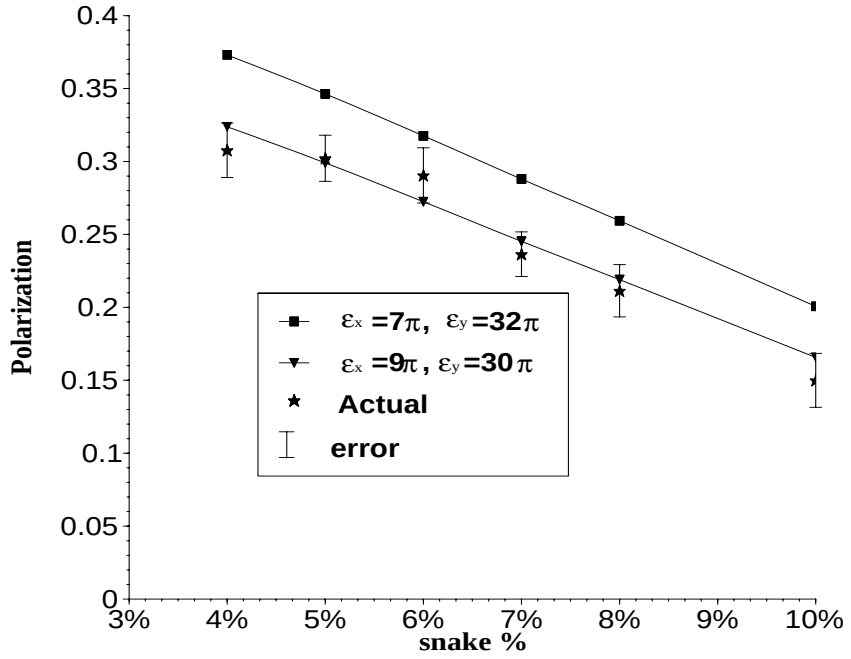

Figure 5.9: Polarization after crossing the $0 + \nu_x$ and $0 + \nu_z$ resonances with fixed vertical tune and horizontal tune ($\nu_z = 8.8$, $\nu_x = 8.7$) scanning from 4 to 10% partial snake strength. Vertical and horizontal emittances were measured to be $(8 \pm 1)\pi$ and $(30 \pm 1)\pi$ mm-mrad for DEPOL calculations. In addition a distributed roll was applied to the BD and CF magnets as described in this section.

Chapter 6

Three Solutions to Reduce Depolarization in AGS

There are three major types of resonances observed in the AGS, imperfection, intrinsic and coupled. Imperfection resonances have been cured using a 3-5% partial solenoid snake [21], and the strong intrinsic resonances using an ac dipole [14]. However the solenoid snake has introduced a strong linear coupling spin resonance which still remains to be dealt with. Using the software described in the previous chapters we consider three techniques to minimize the effect of both the weak intrinsic and coupled spin resonances.

6.1 The AGS Intrinsic Resonance Structure

It is useful to understand the behavior of the dominant $\rho z''$ term in the resonances integral Eq. (2.28). The resonance strength can be approximated by

$$\varepsilon \approx -\frac{1+G\gamma}{2\pi}\oint z''e^{iK\theta}ds = +\frac{1+G\gamma}{2\pi}\oint k_z(s)ze^{iK\theta}ds. \tag{6.1}$$

Here we have used the homogeneous equation $z'' = -k_z z$. For intrinsic resonance we can use the equation for betatron motion and Eq. (6.1) becomes,

$$\varepsilon \approx \frac{1+G\gamma}{2\pi}\sqrt{\frac{\epsilon_N}{\pi\gamma}}\oint k_z(s)\sqrt{\beta_z(s)}\cos(\nu_z\phi_z(s))e^{iK\theta}ds. \tag{6.2}$$

Here β the betatron function, ϵ_N the normalized emittance, ϕ the betatron phase and θ the angular location in the ring.

The AGS lattice is made up of twelve super-periods each containing twenty combined function magnets of long and short lengths. In Fig. 6.1 a graphical representation of the lattice is shown. The resulting structure proves fairly complex. But some general observations are possible. The lattice can be broken down into two sections which are anti-symmetric. Further these sections can be broken down into a total of four sections of two anti-symmetric pairs. There are also two mirror symmetric pairs. While clearly the overriding periodicity of 12 places all our intrinsic resonances at $12n \pm \upsilon_z$, the anti-symmetric structure can explain the odd and even substructure of the resonances. This explanation follows in a manner similar to the evaluation of a typical FODO lattice structure. In a standard FODO lattice the Focusing and Defocusing elements (which are anti-symmetric pairs) can contribute additively to the spin

kick when the resonance is odd (n = odd) [22].

Applying this logic to the AGS lattice we can see that the middle two anti-symmetric pairs can be viewed as having an overall sign difference when seen as a whole. The same is true for the outer two anti-symmetric pairs. For the AGS we know that $\phi \approx \theta$ so between the anti-symmetric pairs there will always be phase difference of $(K \pm \nu_z)\frac{m\pi}{12}$. Here m is some integer determined by which pair is being counted. So at the intrinsic resonance where $K = 12n \pm \nu_z$, the anti-symmetric elements should contribute additively to the spin kick when n is odd and subtract when n is even. This explains why we see in Table 1 that the odd resonances tend to be larger than the even ones (except when $n = 0$).

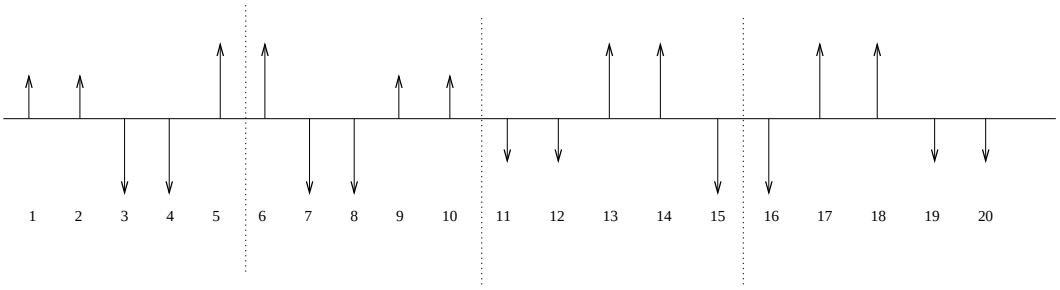

Figure 6.1: AGS superperiod. Here the up and down vectors show the direction and magnitude of the focusing gradients.

6.1.1 Suppression of the Weak Intrinsic Resonances

The complexity of the lattice seems to prohibit a real increase in the super-periodicity of the lattice without significant and costly re-modifications. While there exist many points of overall mirror symmetry, it is clear that neither a single nor several quadrupoles can increase the overall periodicity. If we approach

γ	Gγ	Re(ε_k)	Im(ε_k)	$\mid \varepsilon_k \mid$
4.871	0+υ	0.006128	-0.000271	0.00613421
8.515	24-υ	0.000240	0.000011	0.00023988
11.565	12+υ	0.000094	0.002118	0.00211998
15.208	36-υ	-0.000248	0.005589	0.00559465
18.258	24+υ	0.000507	-0.000022	0.00050779
21.902	48-υ	0.000652	0.000029	0.00065232
24.951	36+υ	0.000479	0.010820	0.01083078

Table 6.1: Resonance strengths ε_k as calculated by DEPOL for the bare AGS machine using the rms emittance for a 10 π mm-mrad beam.

the problem from a purely spin matching aspect then it seems that individual resonances can be suppressed with a well placed family of quadrupoles. Since our resonance structure shows that the $12n \pm \upsilon_z$, n=even resonances are primarily real and the n=odd are primarily imaginary, a family of quadrupoles of the right strength and phase location could suppress individual resonances.

Since the strength and location of resonances are tied to the symmetry of each super-period and the periodic structure of the lattice, one strategy to suppress or enhance a resonance is by the careful placement and field strength setting of quadrupole elements. It is well known that in certain instances using carefully placed families of quadrupoles it is possible to suppress individual resonances by the introduction of a countervailing perturbation to the resonance strength which can be approximated by [22],

$$\Delta\varepsilon_k = (\frac{1+G\gamma}{4\pi})\sqrt{\frac{\epsilon_N}{\pi\gamma}}\int \Delta g(s)\sqrt{\beta}(e^{i(\nu\varphi-k\theta)} + e^{-i(\upsilon\varphi-k\theta)})ds. \qquad (6.3)$$

We use $\Delta g(s) = \frac{1}{B\rho}\frac{\partial B_z}{\partial x}$ as the focusing strength. This equation will give a good

approximation providing that both $\Delta g(s)$ and $\Delta\beta(s)$ are small. It seems that if we use just the right field strengths and locations, we can use this perturbation to cancel our existing resonance. This is known as spin matching.

It might prove insightful if we try to develop an analytical approximation to Eq. (6.3) If we consider the effect of only one additional quadrupole per super-period, Eq. (6.3) can be integrated as a sum over the number of super-periods in the lattice. Using a thin lens approximation this series can then be summed using the properties of a geometric series to give,

$$\Delta\varepsilon_k = (\frac{1+G\gamma}{4\pi})\sqrt{\frac{\epsilon_N}{\pi\gamma}}\{e^{i(\upsilon+k)(\frac{P-1}{P})\pi}\zeta_P(\frac{k+\nu}{P})[g_1\sqrt{\beta_1}e^{i(\nu\varphi_1+k\theta_1)}]+ \\ e^{i(k-\upsilon)(\frac{P-1}{P})\pi}\zeta_P(\frac{k-\nu}{P})[g_1\sqrt{\beta_1}e^{i(k\theta_1-\nu\varphi_1)}]\}. \qquad (6.4)$$

Here θ_1 and φ_1 are the angle and betatron phase at the quadrupole's position. We also assume that we are inserting one quadrupole per superperiod (P).

If we pick the location of the quadrupole wisely then we can control either the imaginary or real part of the resonance. So for example in the AGS where $\theta \approx \varphi$, if we choose the 15th position which corresponds to 22.5° then we can control the real part for all $12n \pm \upsilon$ with n even and the imaginary part for odd n. In principle, provided that there are no other limitations, we can suppress these components of the resonance strength to an arbitrary degree. This is exactly what Lehrach showed in his paper[2] on suppressing intrinsic spin harmonics. We re-confirmed his results in Figs. 6.2 - 6.3 where the $24 \pm \upsilon$ and $48 - \upsilon$ have been successfully suppressed using a family of 12 quadrupoles of identical design as the existing tune quadrupoles.

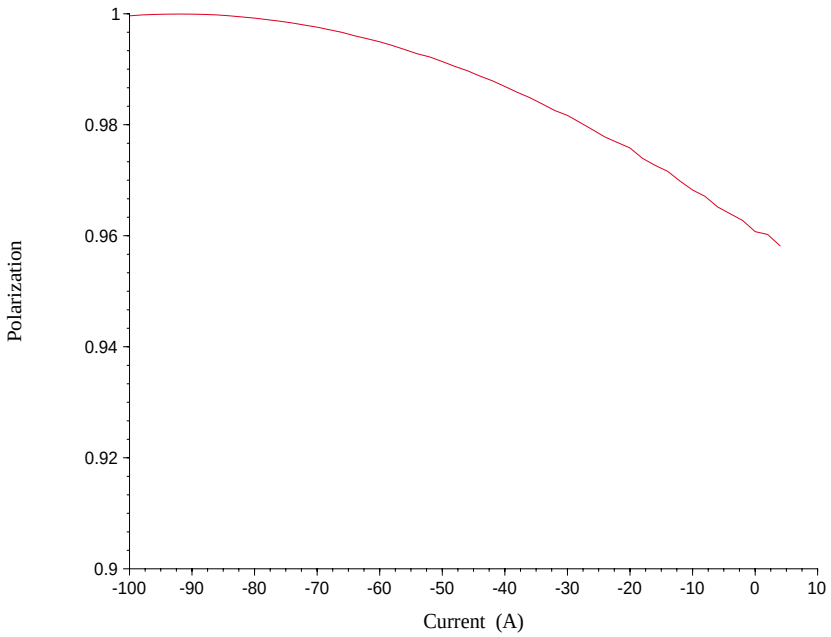

Figure 6.2: Polarization after crossing the $24-\nu_z$ resonance with fixed vertical tune and horizontal tune ($\nu_z = 8.7$, $\nu_x = 8.8$). Scanning currents for a set of hypothetical quadrupoles at the 15th position in the each superperiod. The vertical rms emittance for a 10π mm-mrad beam was used. The acceleration rate was $\alpha = 2.4 \times 10^{-5}$ and snake strength set to 3%.

Considering the use of the AGS's vertical and horizontal tune quadrupoles to effect the weak spin resonances, we find since 24 and 48 yield both imaginary and real resonance contributions these quadrupoles are located at the 3rd ($\varphi = 4.5°$)and 17th ($\varphi = 25.5°$) position in the lattice. If both the horizontal and vertical quadrupoles were activated at once, a configuration could be constructed where either the imaginary or real part of the perturbation would cancel out leaving only a single real or imaginary component. However

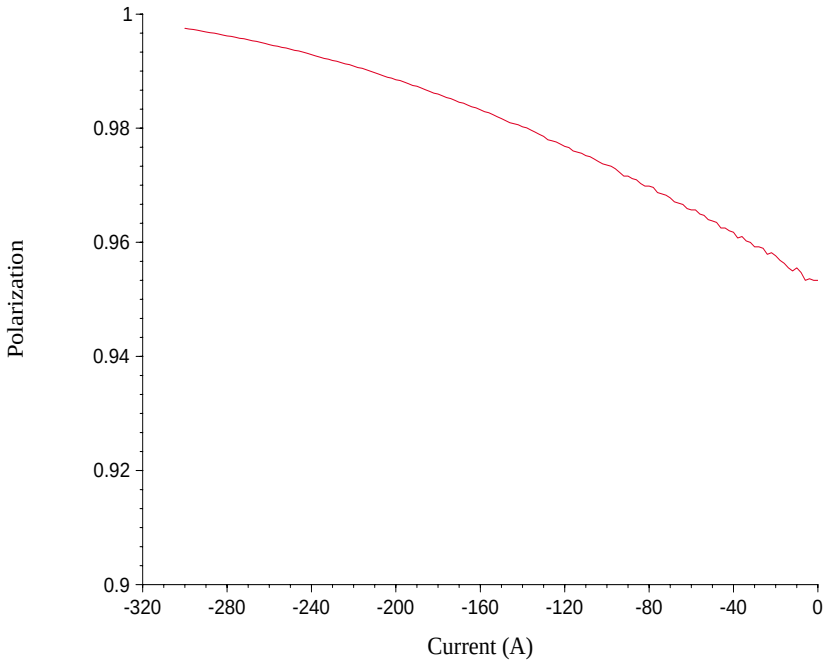

Figure 6.3: Polarization after crossing the $24+\nu_z$ resonance with fixed vertical tune and horizontal tune ($\nu_z = 8.95$, $\nu_x = 8.6$). Scanning currents for a set of hypothetical quadrupoles at the 15th position in the each superperiod. The vertical rms emittance for a 10π mm-mrad beam was used. The acceleration rate was $\alpha = 2.4 \times 10^{-5}$ and snake strength set to 5%.

the field strength requirements would require leaving the 8.5-9.0 vertical and horizontal tune space and further require a field strength beyond the capacity of the existing quadrupoles.

6.2 AGS Coupled Spin Resonance Structure

The presence of skew quadrupoles, solenoids and closed orbit distortions through sextupoles lead to coupling between the horizontal and vertical betatron os-

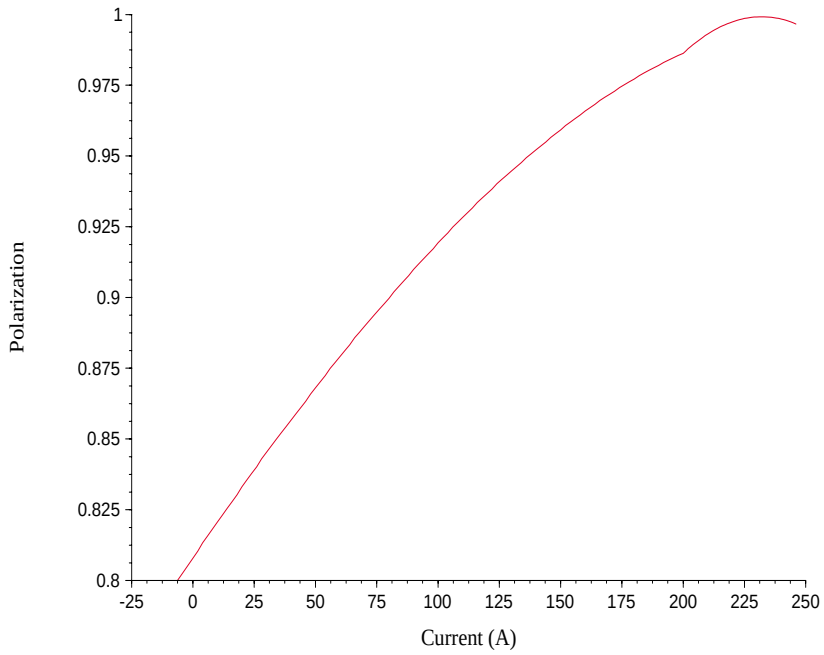

Figure 6.4: Polarization after crossing the $48-\nu_z$ resonance with fixed vertical tune and horizontal tune ($\nu_z = 8.7$, $\nu_x = 8.6$). Scanning currents for a set of hypothetical quadrupoles at the 15th position in the each superperiod. The vertical rms emittance for a 10π mm-mrad beam was used. The acceleration rate was $\alpha = 2.4 \times 10^{-5}$ and snake strength set to 5%.

cillations. In this case vertical betatron motion can be expanded into normal modes. Near a single coupling betatron resonance ($\nu_x - \nu_z = l, l = 0, \pm 1, \pm 2...$) the vertical betatron motion can be approximated.

$$z_\beta \approx \sqrt{\frac{\beta_z \epsilon_z}{\pi}} \cos(\nu_\pm \phi_z + \chi_\pm) + C_x \sqrt{\frac{\beta_x \epsilon_x}{\pi}} \cos(\nu_\pm \phi_x + \chi_\pm) \qquad (6.5)$$

Where $\nu_\pm$ are the normal mode tunes given by

$$\nu_\pm = \frac{1}{2}(\nu_x + \nu_z \pm l) \pm \frac{1}{2}\lambda, \quad \lambda = \sqrt{(\nu_x - \nu_z - l)^2 + |C_-|^2} \tag{6.6}$$

and the coupling coefficient is given by

$$C_x = \frac{|C_-|}{|\nu_x - \nu_z - l| + \lambda} \tag{6.7}$$

with

$$C_- = \frac{1}{2\pi} \oint \sqrt{\beta_x \beta_z} A_{xz} e^{i(\nu_x \phi_x - \nu_z \phi_z - (\nu_x - \nu_z - l)s/R)} ds. \tag{6.8}$$

Here $\phi_{x,z}$ are the horizontal and vertical betatron phases respectively, R is the average radius of the accelerator, and A_{xz} is given by

$$A_{xz} = \left\{ \frac{\frac{\partial B_x}{\partial x}}{B\rho} + \frac{B_\parallel}{2B\rho} \left[\left(\frac{\alpha_x}{\beta_x} - \frac{\alpha_z}{\beta_z} \right) + i \left(\frac{1}{\beta_x} + \frac{1}{\beta_z} \right) \right] \right\} \tag{6.9}$$

where $\frac{1}{B\rho}\frac{\partial B_x}{\partial x}$ is the skew quadrupole gradient, $B_\parallel$ is the solenoid field strength, and $\alpha_{x,z}$ are the usual Twiss parameters.

Since resonances are in general due to spin coherent oscillations in the vertical plane, we can see from Eq. (6.6) that the introduction of a horizontal frequency in the vertical plane will yield a new resonance associated with the horizontal tune. The strength of this coupled spin resonance will be a function of the coupling coefficient, which itself is a function of the strength of the distributed coupling elements in the lattice and the distance between the horizontal and vertical tunes.

Clearly a strategy for reducing the effect of coupled spin resonances should

γ	Gγ	Re(ε_k)	Im(ε_k)	$\mid \varepsilon_k \mid$
4.871	0+ ν_x	0.000750068	0.000985029	0.001238064
11.565	12+ ν_x	-0.000293056	0.000268527	0.000397626
15.208	36- ν_x	0.000846892	0.000620968	0.001050869
24.951	36+ ν_x	-0.001736388	0.001412348	0.002238584

Table 6.2: Coupled Spin Resonance strengths ε_k as calculated by DEPOL for the bare AGS machine with a 5% snake and including distributed roll applied to the BD and CF magnets as outlined in Chapter 5. The rms emittance for a 10 π mm-mrad beam was used.

include maintaining maximal separation between the horizontal and vertical tunes. Additionally it is possible that introducing countervailing coupling elements to cancel the effects of existing coupling can further reduce the strength of the coupling coefficient. In the case of the AGS it might be possible to reduce or eliminate coupling induced by the solenoidal snake using the existing skew quadrupoles plus a second family of skew quadrupoles powered at the right strength.

6.2.1 Suppression of the Coupled Spin Resonances

The AGS already is equipped with six skew quadrupoles located in the 17th location at every other super period. To globally decouple the AGS ideally one should pick a location with as large a phase difference from the existing skew quadrupoles. Unfortunately we are limited in the number of free locations. The 15th location which has been suggested for the future normal quadrupole could also accommodate a skew quadrupole.

Unfortunately the field strength required to approach a situation of global

decoupling causes a large tune shift in the AGS which makes identifying the proper strengths necessary to decouple the machine difficult if not impossible. However since we are concerned with eliminating the coupled spin resonances and not necessarily decoupling the AGS a spin matching condition similar to what was observed with the weak intrinsic resonances is possible. In Figs. 6.5-6.8 we have fixed our vertical and horizontal tunes ($\nu_z = 8.8, \nu_x = 8.7$) and scanned through various current strengths for the 15th and 17th skew quadrupoles. For all four resonances a solution appears possible, however overcoming the $36 + \nu_x$ requires a current in excess of 1200 A. This high current might prove difficult but since it needs to be maintained only during the brief milliseconds of the resonance crossing it should be possible. All calculations were done assuming the 15th skew quadrupole would be identical to the existing 17th skew family.

Actually since the calculations were all done using the slower acceleration rate of $\alpha = 2.4 \times 10^{-5}$ generated by the old backup Westinghouse power supply, and not the usual $\alpha = 4.8 \times 10^{-5}$ which is normally achieved by the Siemens power supply depolarization could effectively be overcome with a stronger residual resonance.

6.3 The Strong Partial Snake Experiment

The presence of a partial snake of strength r modifies the spin ν_s according to

$$\cos \pi\nu_s = \cos \frac{r\pi}{2} \cos G\gamma\pi. \tag{6.10}$$

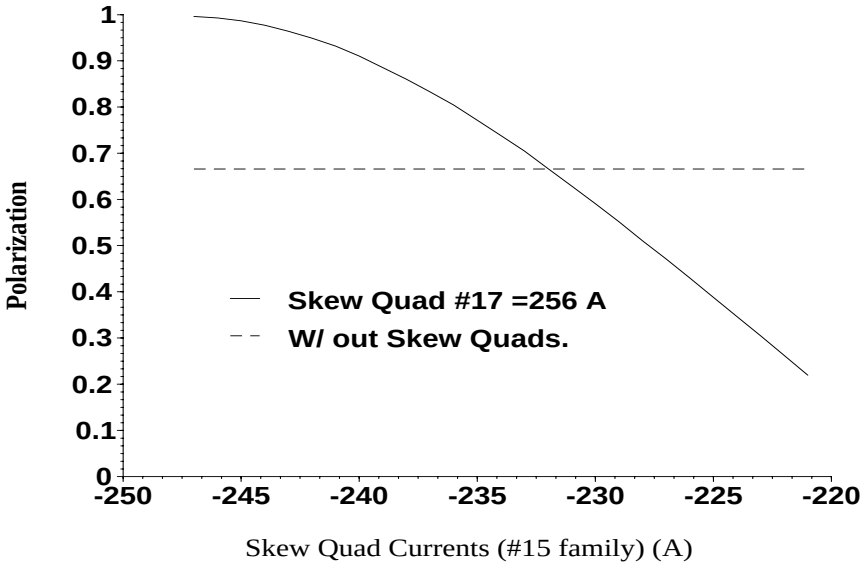

Figure 6.5: Polarization after crossing the $0 + \nu_x$ resonance with fixed vertical tune and horizontal tune ($\nu_z = 8.8$, $\nu_x = 8.7$). Scanning currents for a hypothetical skew quadrupole in the 15th lattice position and the 17th skew quadrupole family fixed at 256 A. The vertical rms emittance for 95% of a 10 π mm-mrad beam was used. The acceleration rate $\alpha = 2.4 \times 10^{-5}$ and the snake strength set to 5%.

Normally with a full snake $r = 1$ thus forcing the spin tune to be 0.5, however when r is small the spin tune returns to its original energy dependency becoming nearly equal to $G\gamma$. However when $G\gamma$ becomes an integer the spin tune ν_s encounters a discontinuity and the spin tune will jump from $-r/2$ to $+r/2$ skipping the imperfection resonance condition. In this way all imperfection resonances can be avoided provided that the resonance strength is much smaller than the gap this discontinuity creates.

Clearly as the partial snake strength s increases the gap around the integer $G\gamma$ value increases. It has been proposed [22] that if this gap was wide

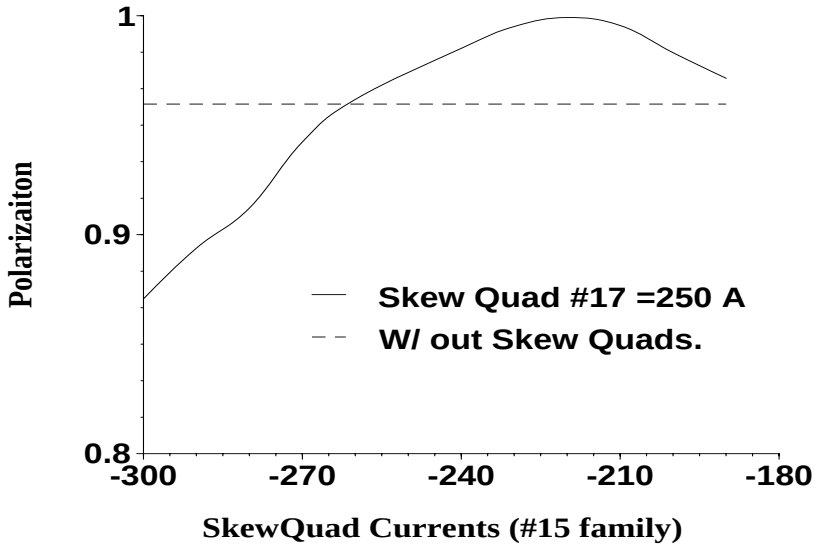

Figure 6.6: Polarization after crossing the $12+\nu_x$ resonance with fixed vertical tune and horizontal tune ($\nu_z = 8.8$, $\nu_x = 8.7$). Scanning currents for a hypothetical skew quadrupole in the 15th lattice position and the 17th skew quadrupole family fixed at 250 A. The vertical rms emittance for a 10 π mm-mrad beam was used. The acceleration rate was $\alpha = 2.4 \times 10^{-5}$, and the snake strength was set to 5%. (Note the wiggle in the curve is due to an occasional failure of the MAD program to find the set tunes.)

enough the intrinsic resonances could be "driven" through this gap. That is, if the vertical betatron tune were close enough to the integer, this gap would encompass all intrinsic resonances and provide a method to overcome them.

Obviously the ideal solution to the problem of depolarization in the AGS would be the installation of a full Siberian snake; however there are no available straight sections in the AGS which could accommodate a full Siberian snake. A compromise would be the installation of a strong partial snake which would create a gap in the tune space large enough to place the vertical betatron tune

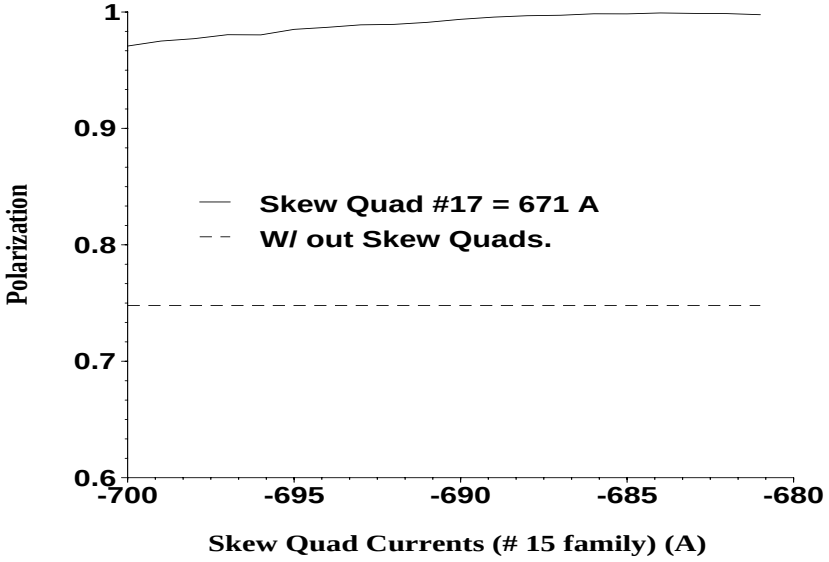

Figure 6.7: Polarization after crossing the $36-\nu_x$ resonance with fixed vertical tune and horizontal tune ($\nu_z = 8.8$, $\nu_x = 8.7$). Scanning currents for a hypothetical skew quadrupole in the 15th lattice position and the 17th skew quadrupole family fixed at 671 A. The vertical rms emittance for a 10 π mm-mrad beam was used. The acceleration rate was $\alpha = 2.4 \times 10^{-5}$, and the snake strength was set to 5%.

inside yet still avoiding beam instability associated with the integer stop-band. This was recently studied (see Ref. [23]) and is now being actively developed.

6.3.1 Results

The efficacy of a strong partial snake was tested using the existing partial solenoidal snake in the AGS. The spin rotation induced by the solenoid is given by

$$\phi = e(1+G)\mu_0 NI/cp, \tag{6.11}$$

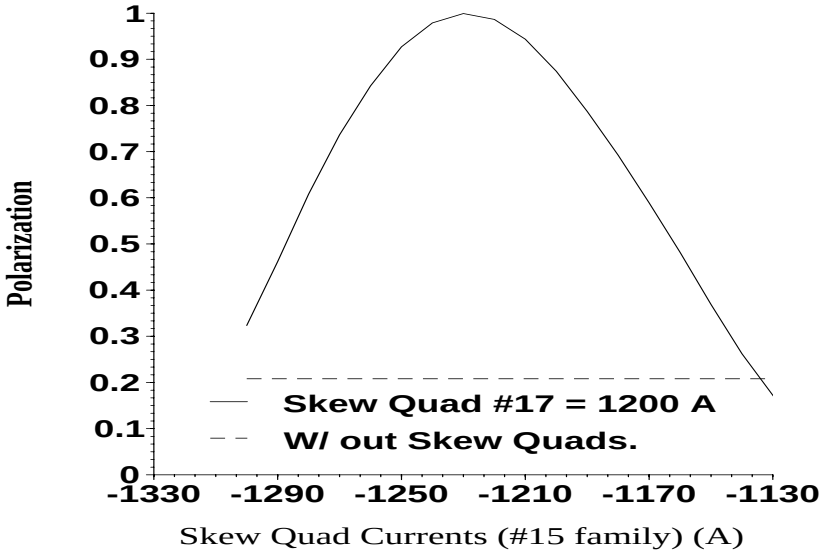

Figure 6.8: Polarization after crossing the $36+\nu_x$ resonance with fixed vertical tune and horizontal tune ($\nu_z = 8.8$, $\nu_x = 8.7$). Scanning currents for a hypothetical skew quadrupole in the 15th lattice position and the 17th skew quadrupole family fixed at 1200 A. The vertical rms emittance of a 10 π mm-mrad beam was used. The acceleration rate was $\alpha = 2.4 \times 10^{-5}$, and the snake strength was set to 5%.

where p is the momentum of the proton beam, μ_0 is the permeability of the vacuum, and NI is the current times the number of turns turns. The effective snake strength becomes $s = \phi/\pi$. Since the analyzing power of the AGS polarimeter and the strength of solenoidal snake both fall off with increasing energy, we examined the crossing at the lowest intrinsic resonances $G\gamma = 0+\nu_z$. At this energy the solenoid can generate a 25% snake, however with a stronger solenoidal field comes stronger coupling. A snake strength of 11.4% was chosen for this experiment as a compromise between spin tune gap size and enhanced coupling spin resonances. The horizontal tune was kept at 8.54 while the

vertical tune was raised to 8.98. At this vertical tune the orbit had to be carefully corrected to reduce the beam instabilities near the integer stop-band.

The results of the experiment are shown in Fig 6.9. At the top vertical tune the discrepancy between injection and measured polarization can be attributed to the remaining coupled spin resonance and the new direction of the spin closed orbit, which under the influence of the partial snake has shifted 20.52° by the 11.4% snake. Of particular interest is the dip in polarization near $\nu_z = 8.97$. This is believed to be due to the existence of a second order snake resonance ($l = 2$) since the spin tune $\nu_s = 0.057$ for an 11.4% snake near $G\gamma \approx 9$. By Eq. (2.31) a second order snake resonance should exist at $\delta\nu_z = 0.9715$. This snake resonance reduces the available tune space making the selection of operating tunes even more critical. Furthermore since we are dealing with an even order snake resonance much care must be take with vertical closed orbit corrections, since a bad closed orbit will expand the snake resonance as well as hurt beam stability near the integer stop-band.

There are several advantages to using a strong partial snake. First the strong partial snake will allow us to avoid all imperfection, weak and strong intrinsic resonances. Additionally its operation should avoid some of the problems associated with the operation of the ac dipole which has required constant monitoring and care, due to slight current fluctuations in the tune quadrupoles and the general nonlinear response of the net spin-flip. The ac dipole also causes beam loss due to scrapping at the $0 + \nu_z$ crossing. If this could be avoided the overall intensity transfered to RHIC could be improved. Finally coupled spin resonances could be dealt with by either pushing the horizontal and vertical tunes through the spin tune gap, or a new family of skew

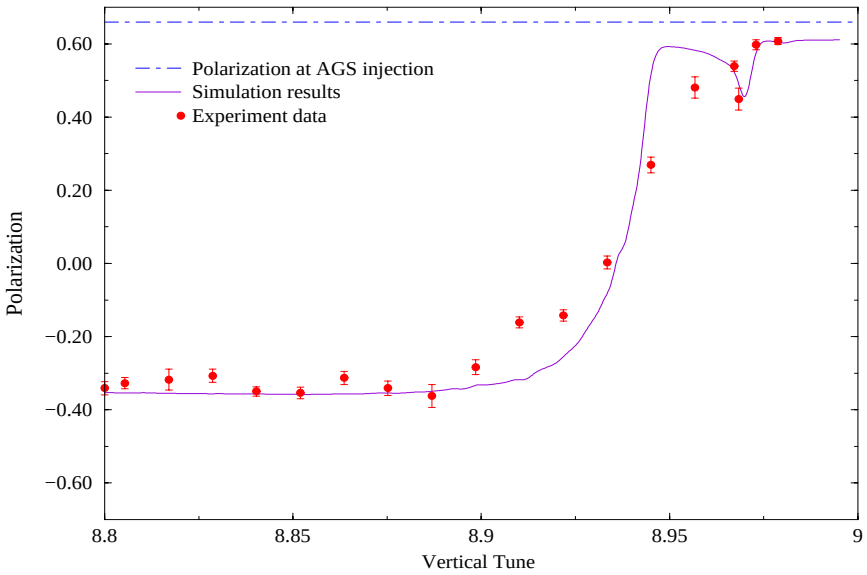

Figure 6.9: The measured vertical polarization as a function of the vertical betatron tune for an 11.4% partial snake. The dots are measured polarization, and the error bars only represent the statistical errors. The dashed line is the polarization level measured at the end of the LINAC. The solid curve is the simulation result using both the new DEPOL and a tracking model with two overlapping resonances. This figure was taken from [23].

quadrupoles could be added to eliminate the coupled spin resonances.

The design of a new super-conducting helical partial snake to replace the solenoidal snake is currently underway. It is believed that a 20% to 30% partial snake should be sufficient to overcome intrinsic resonances at all energies. The helical design will minimize the effective coupling induced by the partial snake.

Chapter 7

The Configuration of RHIC

RHIC receives polarized protons at $G\gamma = 46.5$ and accelerates them up to $G\gamma = 192$ during which it crosses many intrinsic and imperfection resonances. In the RHIC lattice, there are six arcs with 12 FODO cells in each arc. Due to the anti-symmetric arrangements, the superperiod is $P = 3$ while the effective number of dipole cells is $M = 27$. This configuration places all the intrinsic resonances at $nP \pm \nu_z$.

To avoid resonances RHIC is equipped with two full Siberian snakes in each ring (Blue and Yellow rings). They are situated on opposite sides of each ring and serve to avoid depolarizing resonances by introducing 180° spin rotation without an associated net orbit distortion. The helical dipole snakes are composed of four separate helical dipoles with a combined total length of 10.56 m [24]. The outer and inner two magnets are powered on the same power supply but with opposite polarity. The effect of the snakes is to keep the spin tune equal to 1/2 during acceleration thus avoiding the intrinsic and

imperfection resonance condition. However depolarization can occur through the snake resonance condition.

During the 2002 polarized proton run the AGS typically delivered protons polarized at 25%. RHIC was able with the help of the snakes to maintain this polarization during the ramp up to 100 GeV for many of the fills. However on several occasions the polarization transfer efficiency dropped well below 100% due to crossing the 1/4 snake resonance or the 3/14 coupled snake resonance.

In RHIC the primary source of coupling comes from rolls in the triplet quadrupoles at the six interaction regions. In addition the helical dipole snakes introduce a small longitudinal field and the existence of 5 T-m solenoidal magnets field at two of the experiments during a store can further contribute to coupling in RHIC. The solenoidal magnets however are not turned on until flattop is reached. Much effort has been devoted to compensate for the rolls in the triplet quadrupoles through a system of local and global corrections outlined in [20]. These efforts produced some success at injection and flattop. However, problems during the acceleration ramp persisted since a dynamic correction technique has yet to be implemented.

7.1 Snake Field Measurement and Calibration

A lot of work has been done predicting the field structure of the newly installed helical snakes and rotators in RHIC. Analytical[25] [26] [27] [29] and numerical [28] work has been conducted to generate an appropriate model for these elements. But up to now actual field measurements taken from the real magnets have not been analyzed. A comparison of the actual field values with

current analytical models proved problematic in terms of fitting. In addition to the problem of modeling the end effects and accounting for the quadrupole fields, we found a general longitudinal dependence for the multipoles in the helical basis. Since this longitudinal dependence could not be accounted for in a neat analytical solution and required resorting to a series solution expansion we decided that using an available finite element analysis program would be a more efficient method to generate a solution.

However current finite element analysis programs are designed to solve Laplace's equation for cases with a scalar potential boundary condition. Since we possessed multipole data appropriate for the generation of B_ρ field components along a 3.1 cm radius, we needed to develop a magnetic scalar potential along a cylindrical surface in order to use the software to solve the interior field problem. Considering that the B_ρ component must satisfy Laplace's equation separately,

$$\nabla^2 B_\rho = 0. \tag{7.1}$$

We can use TOSCA [30] to solve this version of Laplace's equation thus giving B_ρ everywhere interior to our boundary conditions ($\rho_0 = 3.1$ cm). Using this B_ρ we can evaluate the real magnetic scalar potential Φ_M using,

$$\Phi(\rho_0)_M = \int_0^{\rho_0} B_\rho d\rho + \Phi(0)_M. \tag{7.2}$$

Finally using the derived values for Φ_M we can again use TOSCA [30] as it was intended, generating a useable full field model contained in the OPERA-TOSCA [30] operating environment.

Since we are equipped to solve for fields internal to our known boundary conditions, we are restricted to considering transverse particle motion of $\rho <$ 3.1 cm. Given a beam pipe with an internal radius of 4.5 cm it would be better if we could account for displacements up to at least 4.1 cm. To accomplish this we linearly extrapolated the straight magnetic field formula for B_ρ

$$B_\rho = B_0 \sum_{n=0}^{\infty} \left(\frac{\rho}{\rho_0}\right)^n \left[a_n \cos\left((n+1)\theta\right) + b_n \sin\left((n+1)\theta\right)\right] \tag{7.3}$$

by simply using existing multipole values and evaluating B_ρ at a 4.1cm radius. From Fig. 7.1 it seems clear that using a 4.1 cm radius for the boundary

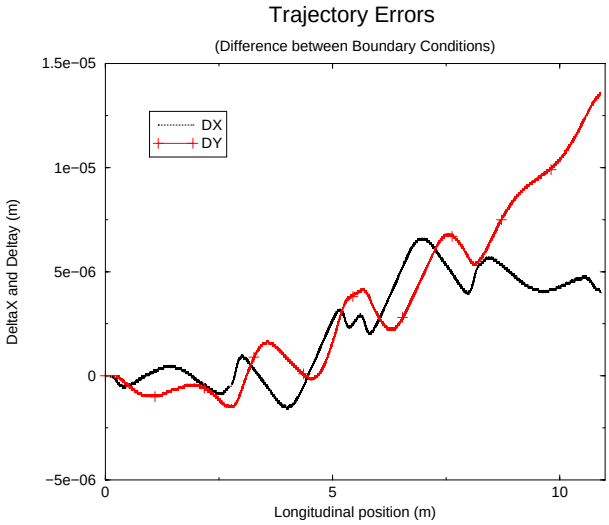

Figure 7.1: Difference in x and y (y is the vertical direction and x horizontal) trajectories for Fields evaluated with boundary conditions at 3.1 cm and 4.1 c.m.

conditions will give reasonable orbit results.

Using SNIG [31] we tracked 100 GeV protons through the field map of

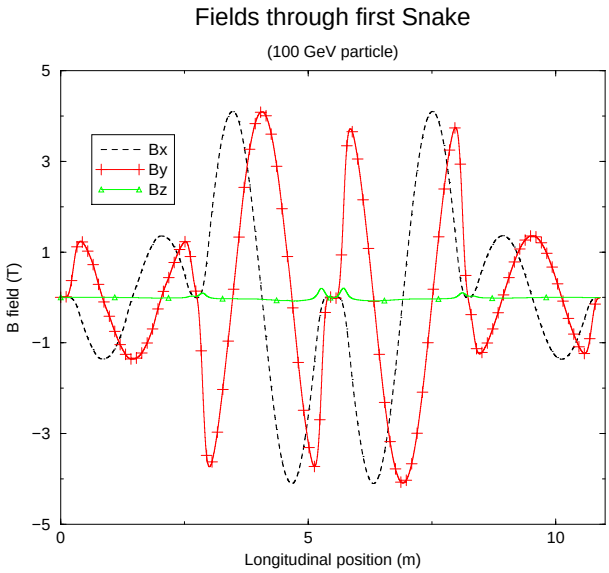

Figure 7.2: B_x , B_y and B_z fields evaluated along 100 GeV particle path.

a single snake with the largest measured deviation (HRD101). Results were consistent with previous predictions; however construction errors lead to exiting orbit displacements of -0.289 mm and -0.489 mm in the x and y direction respectively. In addition the particle picked up angular kicks of -0.46 mrad and -1.21 mrad in x' and y'. Here we now take x to be horizontal direction, y to be vertical and z to be the longitudinal direction for the rest of this chapter. A quick evaluation of the orbit paths for particles entering close to the axis

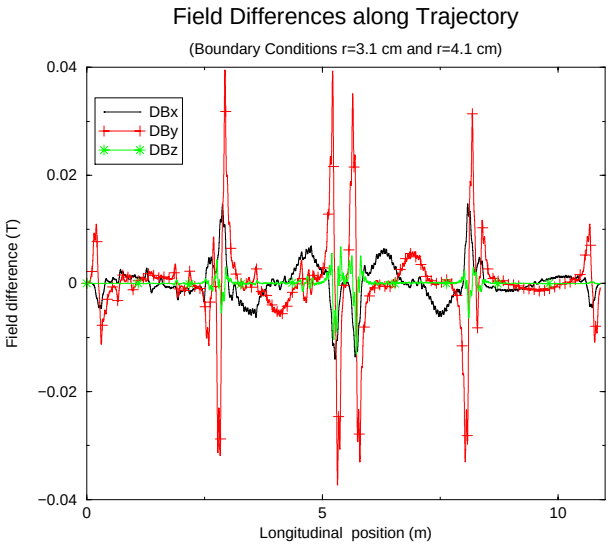

Figure 7.3: ΔB_x , ΔB_y and δB_z fields evaluated along 100 GeV particle path comparing $\rho = 3.1$ cm to a 4.1 cm

with a small transverse momentum yielded the following transfer matrix

$$M = \begin{pmatrix} 0.9964174 & 10.980413 & 0.0014789 & 0.0011432 \\ -0.000656 & 0.9985205 & 0.0002366 & 0.0000774 \\ 0.0001979 & 0.0126185 & 0.9883464 & 10.924713 \\ 0.0002217 & 0.0038101 & -0.002115 & 0.9880669 \end{pmatrix}. \tag{7.4}$$

The determinant for this matrix is $|M| = 1.002$ so for longterm tracking it should be symplectified. From this matrix it is clear that the snakes do induce some coupling. The contribution of this coupling to spin resonances has been evaluated [32] showing a strength on the order of coupling caused by the operation of the solenoidal field in both the PHENIX and STAR detectors yet much less that that caused by the triplet quadrupole rolls at each interaction

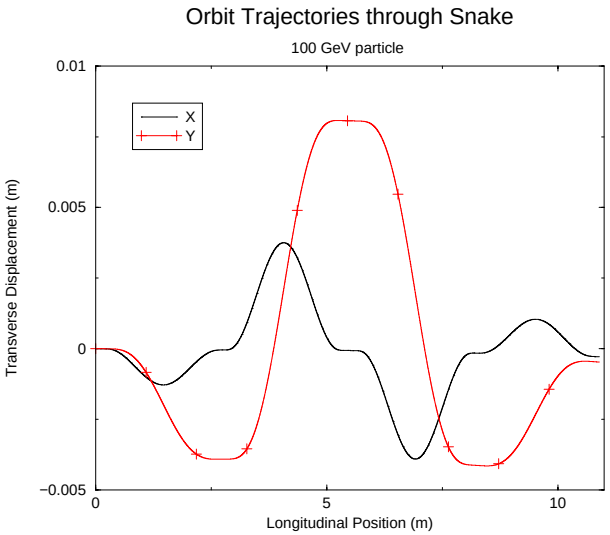

Figure 7.4: X and Y trajectories through full snake.

region.

Considering the behavior of spin through the snake we found our results matched fairly well with previous predictions. With the outer two magnets set at 102 A and the inner two at 329 A the particle achieved a complete spin flip. We now seek to study the spin response of the input currents to the inner and outer helical pairs. It is convenient to parameterize the effects of the snake on the spin by using the angles μ and ϕ. As you can see in Fig. 7.6, ϕ represents the angle between the longitudinal axis in the horizontal plane and the axis of rotation. μ represents the magnitude of the spin rotation about this "snake axis". From the values of μ and ϕ for each snake it is possible to evaluate the total spin tune ν_s of the machine. It is a well known result that ν_s can be

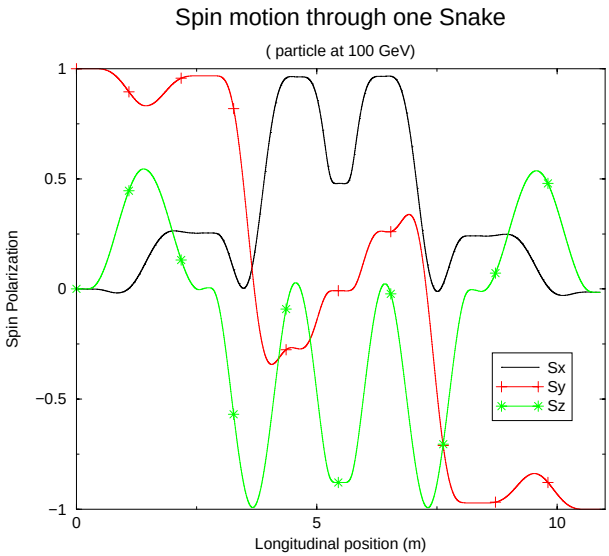

Figure 7.5: $S_xS_yS_z$ Spin trajectories through full snake. Starting off with $S_y = 1$ polarization

given by,

$$\cos \nu_s \pi = \cos \frac{\mu_2}{2} \cos \frac{\mu_1}{2} \cos G\gamma\pi - \sin \frac{\mu_2}{2} \sin \frac{\mu_1}{2} \cos(\phi_2 - \phi_1). \tag{7.5}$$

In order to keep the spin precession energy independent and thus avoid spin resonances it is necessary to keep our spin tune $\nu_s = 0.5$. From Eq. (7.5) it is easy to see that one way this can be accomplished is if the right side is made to vanish. Currently in RHIC the snakes have been configured to achieve this with $\phi_1 = -\phi_2 = \pi/4$ and $\mu_1 = \mu_2 = \pi$.

One of the major challenges has been identifying those settings which can achieve $\mu = \pm\pi/4$ and $\phi = \pi$, the desired snake configuration.

To simplify our predictions we generated μ and ϕ results over a range of

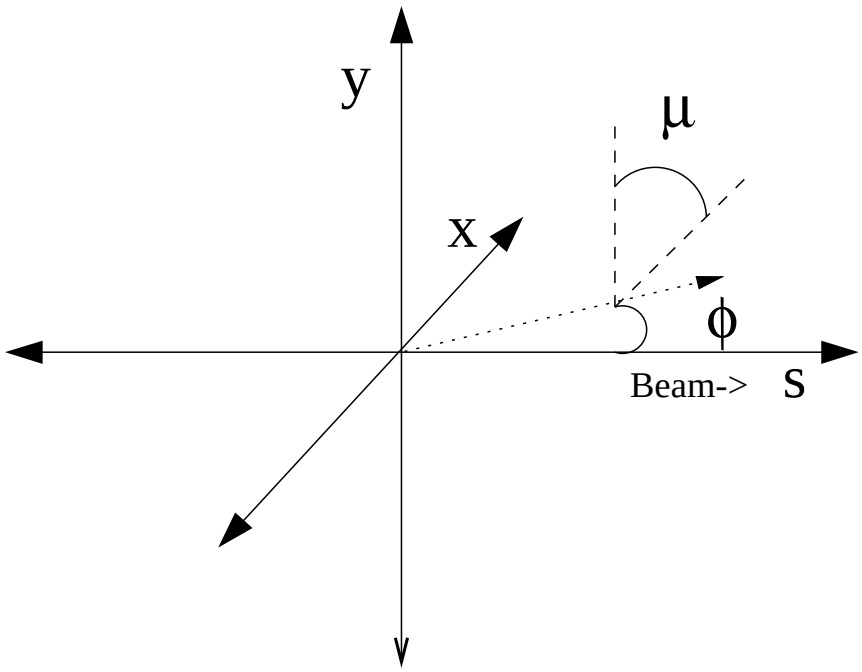

Figure 7.6: Rotation axis of the snake is ϕ and μ is the rotation angle.

input currents and using these constructed a fourth order polynomial fit which was implemented in a simple graphical TCL program. In Figs. 7.7 and 7.8 the residuals from the fit and the actual μ and ϕ values are shown for the snake HRD101(1st snake in blue ring) at $\gamma = 107.0922$. Since most of our data points were collected in the region of $\pm(300-330)$ A for the inner current and $\pm(90-120)$ A for the outer currents our largest residual values naturally occur well outside this range and reach a maximum of $\pm 5^\circ$. Within the operating and detuning range used for the spin flipper commissioning, the deviation is down to less than $\pm 2^\circ$. To achieve the desired $\mu = 180^\circ$ and $\phi = \pm 45^\circ$ values, the RHIC snakes were all powered to 325 A for the inner helices and 100 A on the outer helices. These figures were based on the HRD101 blue snake

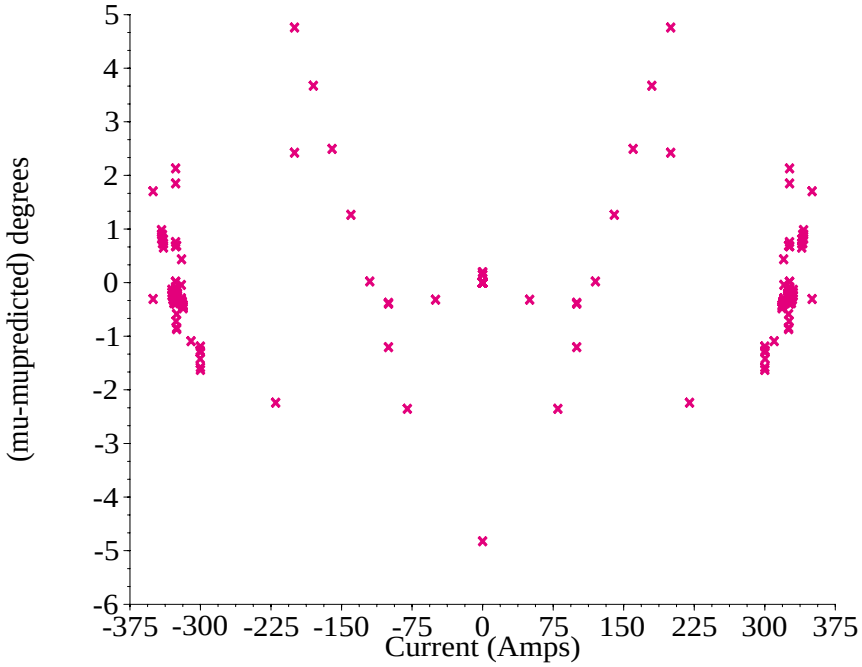

Figure 7.7: μ residuals for snake HRD101 at $\gamma = 107.0922$ versus inner current.

multipole measurements. Since ramping the beam energy from $\gamma = 25.9364$ to $\gamma = 107.0922$ only yielded a 0.01 change in spin tune, the current settings were kept fixed throughout the acceleration ramp.

The process of commissioning the RHIC spin flipper as well provides an estimate of the spin tune. Commissioning of the spin flipper in RHIC is detailed by Bai et,al [33]. Briefly however the driving frequency of the ac dipole was swept through a range where the spin tune was believed to reside. Thus if a spin flip was observed then it was known that the spin tune must lie within the range of frequencies swept by the ac dipole.

Results showed that a partial spin flip (66%) was obtained in the Blue ring when the AC dipole was swept over a driving frequency from 0.47 to 0.49 and

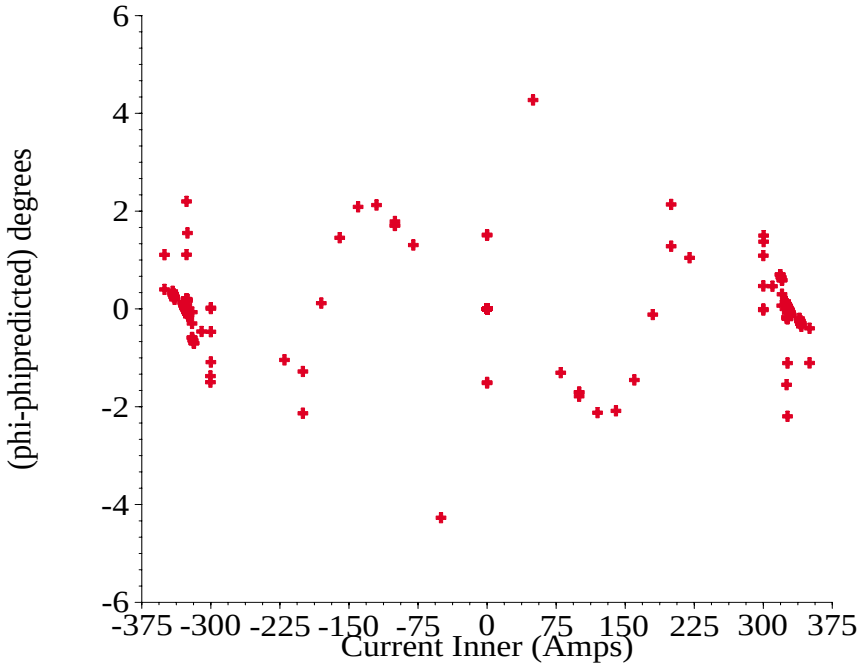

Figure 7.8: ϕ residuals for snake HRD101 at $\gamma = 107.0922$ versus inner current.

the snake was detuned to a predicted value of $\nu_s = 0.48$. These results indicate several possible explanations. Either the spin tune was not exactly 0.48 but on the edge of the 0.47 to 0.49 range or the spin tune spread exceeded ± 0.01.

During this experiment it was noticed that partial spin flipping was observed in the Yellow ring. This was despite the fact that the currents powering the snake were fixed at inner current = 325 A and outer current = 100 A, which by our calculations based on the HRD101 Blue snake should have yielded a spin tune of 0.5. Clearly our spin tune distribution must have partially overlapped with the tunes in the range of 0.47 to 0.49.

If we consider in detail the field strengths of the HRD102 Yellow snake however we find that at the 325 A and 100 A current settings will yield a

$\mu = 179.956475$ and $\phi = -44.0853423$ at $\gamma = 107.0922$. This difference of about 1° can lead to ± 0.01 change in the spin tune which could account for the spin detuning observed in the Yellow ring.

In addition to using the spin flipper it is possible to use snake resonance theory to help estimate the spin tune using the snake resonance condition [7]

$$\delta\nu_y = \frac{\nu_s \pm k}{l}. \tag{7.6}$$

Here l represents the snake resonance order and $\delta\nu_y$ the fractional part of the vertical betatron tune. In the betatron tune space used during the RHIC acceleration ramp tracking indicates that there should be two observable snake resonances, the strongest of which occurs at a betatron tune $\nu_z = 0.25$ [24]. Following from Eq. (7.6) the exact location of this resonance in betatron tune space should be dependent on the exact spin tune achieved by the snakes.

In Figs. 7.9-7.10 we can see graphs of the maximum vertical betatron tune during the acceleration ramp versus polarization transfer efficiency. Clearly in both the blue and yellow rings this snake resonance at $\nu_z = 0.25$ was observed whenever the tune crossed the 0.245 threshold setting a lower bound of 0.49 spin tune for both rings.

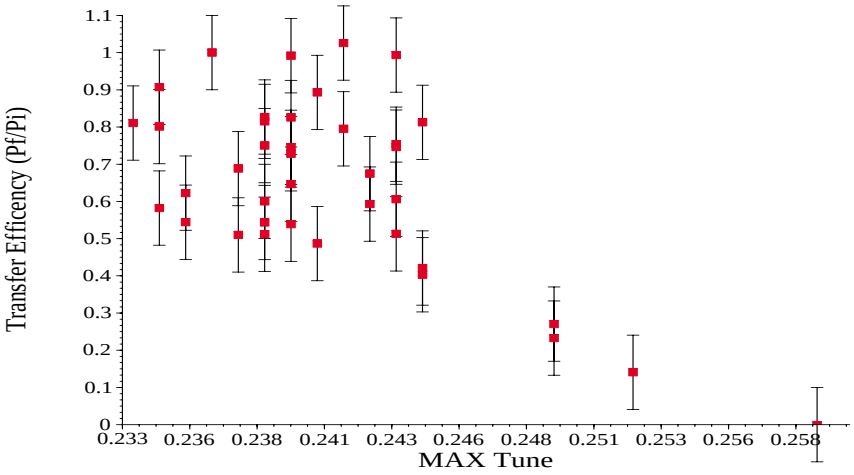

Figure 7.9: Maximum tune along acceleration ramp for Blue ring versus Polarization transfer efficiency (P_f/P_i).

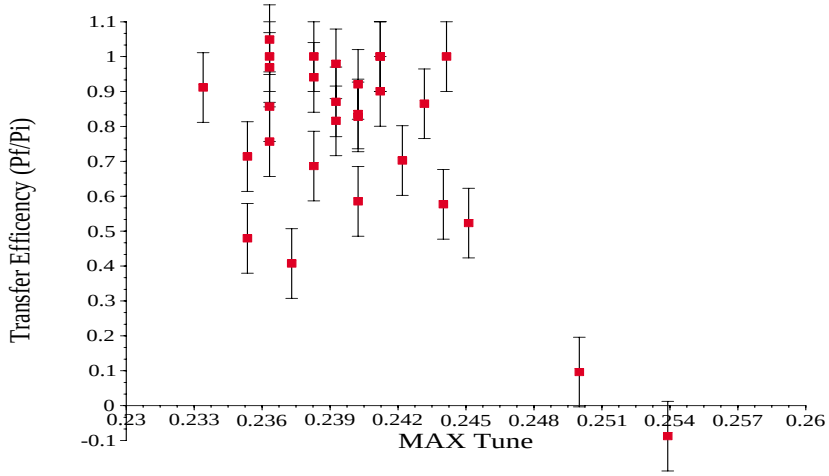

Figure 7.10: Maximum tune along acceleration ramp for Yellow ring versus Polarization transfer efficiency (P_f/P_i).

Chapter 8

Observation of Higher Order Snake Resonances in RHIC

The fractional betatron tune space, in which RHIC was operated during the 2002 polarized proton run ranged from 0.20 to 0.25 with the horizontal tune typically between 0.2 to 0.225 and the vertical between 0.225 to 0.25. Comparisons with the snake resonance graph in Fig. 8.1 shows possible sources of depolarization during the RHIC ramp. Clearly there are three snake resonance locations in betatron tune space that we must worry about: 1/4, 3/16 and 3/14 snake resonances. All snake resonances are seen to split into two peaks.

To rule out the effect of higher order resonances and establish the boundaries for each snake resonance in tune space we calculated the imperfection, intrinsic and coupled spin resonances using DEPOL. The results for the energy range of the RHIC ramp is shown in Fig. 8.2. From the intrinsic and

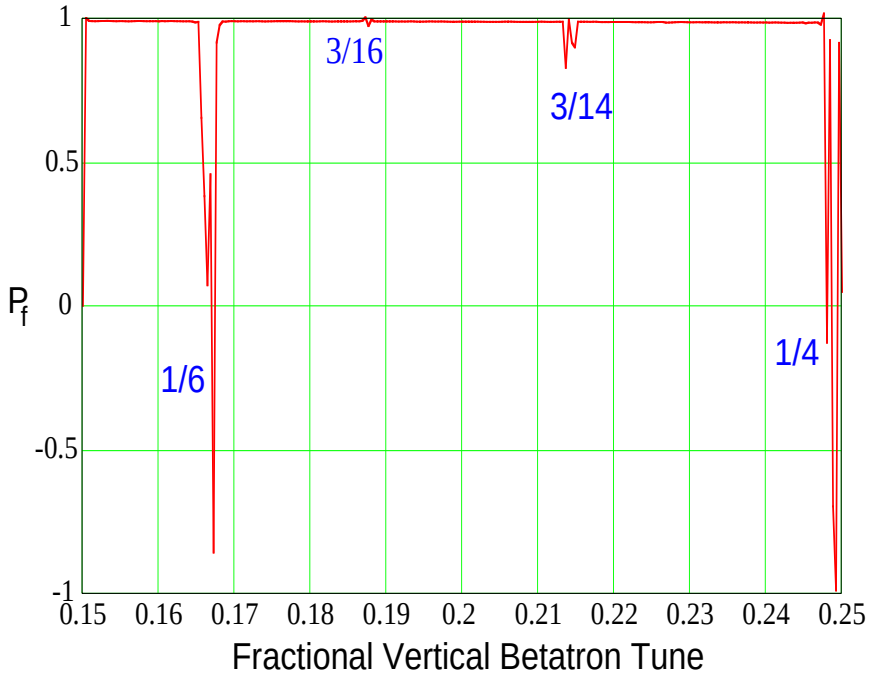

Figure 8.1: Theoretical prediction of the vertical polarization after acceleration through a strong intrinsic resonance of 0.5 and a moderate imperfection resonance of 0.05 shown as a function of the vertical betatron tune. Figure taken from [24].

coupled spin resonance strength calculation, the maximum resonance strength is $\varepsilon_{int} < 0.15$. This precludes the effect of any higher order snake resonances [22]. From the imperfection calculation the maximum imperfection strength $\varepsilon_{imp} < 0.2$ places the maximum tune splitting. Eq. (2.31) places the maximal incursion of 1/4 snake resonances at 0.2424 and for 3/16 at 0.1894. Given the operating tune space we can now rule out the effect of the 3/16 snake resonance.

Thus only the 1/4 and 3/14 snake resonances could have been the source of depolarization during the RHIC ramp. Since the vertical tune during most

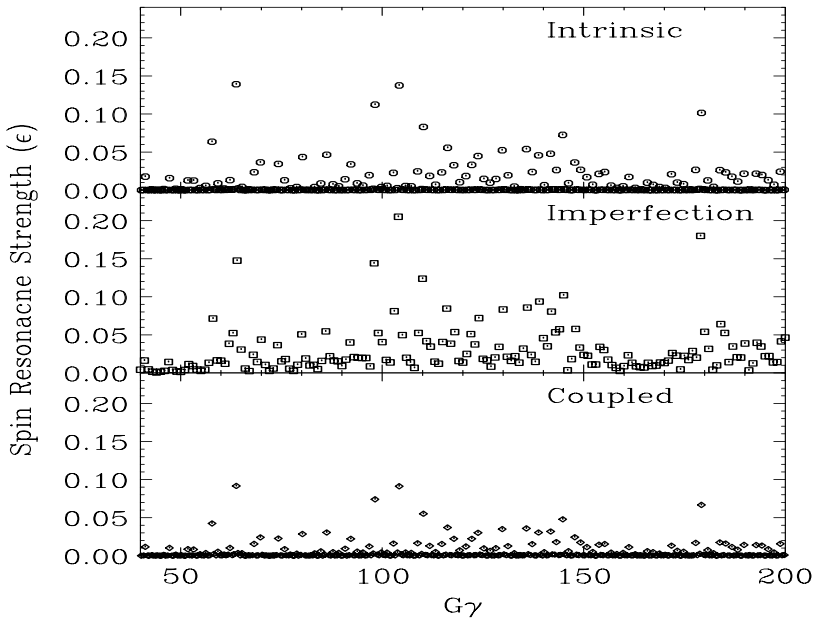

Figure 8.2: Calculated imperfection, intrinsic, and coupled spin resonance strength for RHIC $z_{rms} = 2.2$ mm, using vertical and horizontal emittance of 10π mm-mrad.

of the runs was kept above 29.22, the 3/14 snake resonance from the vertical betatron motion could not have caused depolarization. However, the vertical tune did approach 1/4 on several occasions and the horizontal tune did cross 3/14 on many ramps. An example of the 3/14 coupled snake resonance crossing can be clearly seen from the FFT tune signal shown in Fig. 8.3.

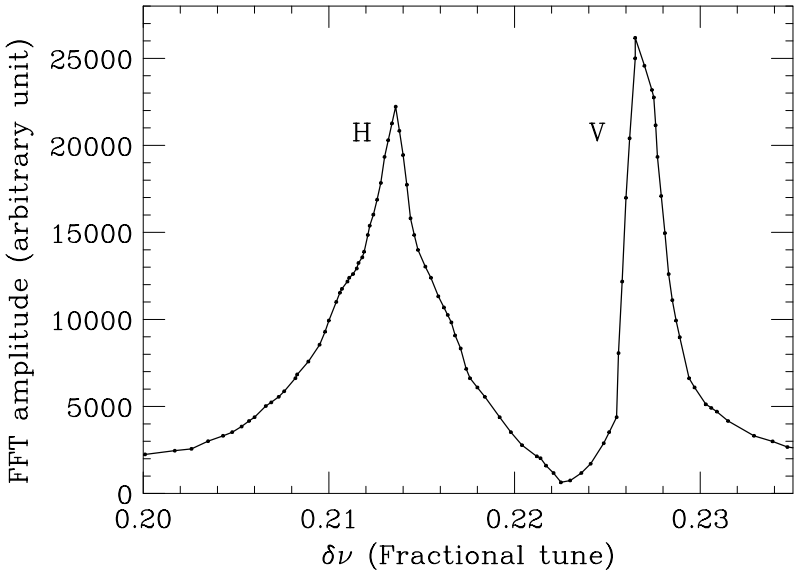

Figure 8.3: Snapshot of the FFT spectrum from the RHIC horizontal tune meter in the Yellow ring. In this ramp the polarization preservation efficiency P_f/P_i dropped to 20%. This snap shot was taken during crossing the second strong resonance location along the RHIC ramp. The double peak is clear evidence of strong coupling, where the horizontal tune (lower peak) is clearly overlapping the 3/14 snake resonance.

Since coupling was evidently significant in RHIC and the horizontal and vertical tunes were run in close proximity, we investigated the significance of the coupled 3/14 snake resonance on polarization. We proceeded by considering the vertical and horizontal tunes at three strong resonance locations along

the RHIC ramp. From these three locations we then selected data for those tunes with both minimum $|3/14 - \nu_x|$ value and $|\nu_x - \nu_z| < 0.02$. From this data we fit a simple Froissart-Stora type of function,

$$< P_f/P_i >= 2e^{-4\pi q} - 1. \tag{8.1}$$

Here q served as a type of resonance strength and was made dependent on both tune separation and distance to the snake resonances,

$$q = \frac{C_1}{|\nu_x - \nu_z|} + \frac{C_2}{|3/14 - \nu_x|} + C_0. \tag{8.2}$$

Linearizing and fitting this equation we found $C_1 = 2.92 \times 10^{-4}$, $C_2 = 5.99 \times 10^{-6}$ and $C_0 = -0.017$ for the blue ring and $C_1 = 2.07 \times 10^{-4}$, $C_2 = 1.47 \times 10^{-5}$ and $C_0 = -0.0144$ for the yellow ring. The R^2 value of the fit for the blue ring is 0.71 and for the yellow ring is 0.74 . Graphs of the 3/14 coupled snake resonance and 1/4 even snake resonance are shown in Fig. 8.4. We can use the resonance widths in Fig. 8.4 to estimate the imperfection resonance strength which perturbed the spin tune at 3/14. For Yellow we found it to be ≈ 0.13 and for blue ≈ 0.095 which means our DEPOL calculations probably overestimated the imperfection resonance strength.

Finally spin tracking results in the Blue ring using the program SPINK [34] and including rolls in the triplet quadrupoles (without correction) show clearly in Fig. 8.5 the onset of the coupled snake resonances as the horizontal tune crosses the 3/14 snake resonance location. What is of interest here is why this resonance fits the Froissart-Stora type function so well. A nice analyti-

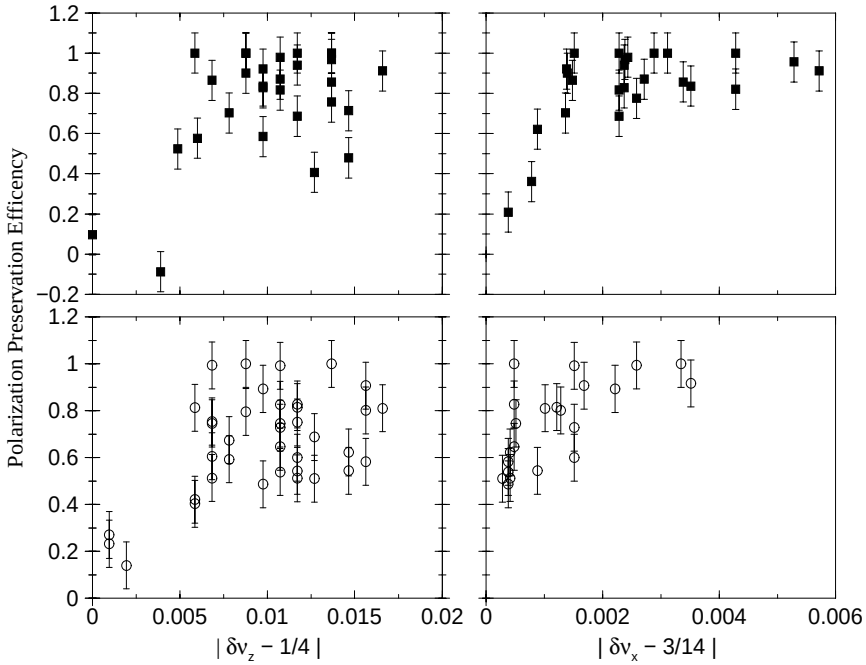

Figure 8.4: $|\delta\nu_z - 1/4|$ and $|\delta\nu_x - 3/14|$ versus polarization preservation efficiency (P_f/P_i) shown for the Yellow (square symbol) and Blue (open circles) rings. In the case of $|\delta\nu_z - 1/4|$, polarization preservation efficiency was scattered between 1.0 and 0.4. This is because for each RHIC fill other machine parameters were fluctuating.

cal prediction for the magnitude of depolarization during a snake resonance crossing does not exist. However the success of this simple model leads one to speculate that perhaps a simple model could be used to at least approximate their behavior. Clearly more theoretical work should be pursued in this vein.

Depolarization due to the 1/4 snake resonance was much easier to show since it is such a strong resonance operating independent of coupling. The left two graphs in Fig. 8.4 clearly show the onset of this snake resonance. As in

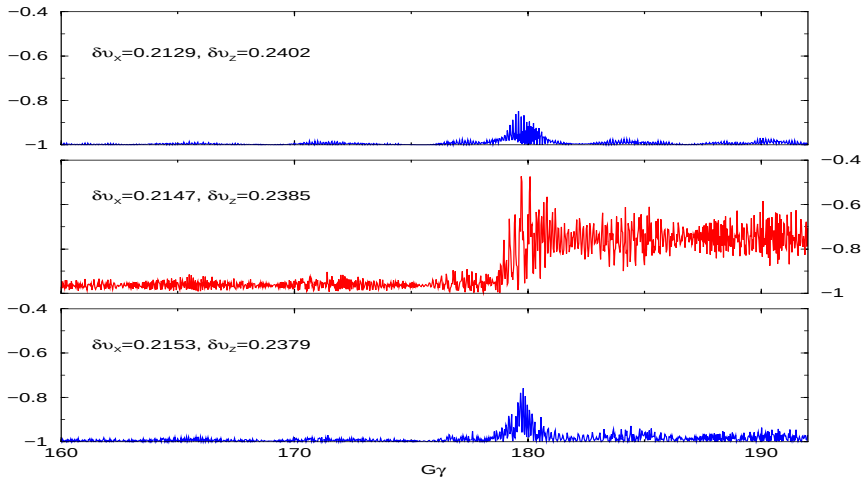

Figure 8.5: Spin Tracking results for strongly coupled Blue ring with an emittance of 25 mm-mrad and $z_{rms} = 0.6$ mm. The three graphs show Polarization versus $G\gamma$ with the fractional part of the horizontal betatron tunes near 3/14. Figure obtained from [35].

the 3/14 case we can use these graphs to estimate the imperfection resonance strength. For both rings we find the imperfection resonance to be about 0.16. Both estimates from the 3/14 and 1/4 snake resonance appear consistent with our DEPOL calculated resonance strength.

Chapter 9

Conclusion

The polarization transfer efficiency of the AGS presents the most clear challenge to achieving higher levels of polarization at top energy in RHIC. The problems in the AGS are centered around the remaining weak intrinsic resonances and the coupled spin resonances. Our studies have shown that several viable solutions exist.

For the weak intrinsic resonances one solution proposed in the past [2] has been reconsidered, namely the addition of a new quadrupole family in the 15th position of each superperiod to cancel the weak intrinsic resonances. This solution has been shown to work theoretically but has yet to be tested in the AGS.

Another solution for the problem of weak intrinsic resonances is the use of a strong partial snake. During the 2002 polarized proton run, for the first time, an 11.4% partial snake was used to effectively over come the strong intrinsic resonance at $0 + \nu_z$. Also for the first time partial snake resonances

were observed confirming previous theoretical predictions [22]. In this case the theory has been well tested; however much care must be taken in its design and execution. Of critical concern is control over the closed orbit errors for three major reasons. First since correction of the intrinsic resonance requires operating the vertical machine tune close to an integer, the existence of orbit errors will make beam stability difficult. Second the existence of an even order snake resonance in this tune space means that the available tune space will be severely limited by the enhancement and splitting of the even order snake resonances in the presences of closed orbit errors. Third since it is necessary to build the partial snake in such a limited space, the field strengths necessary to generate the targeted 20% - 30% partial snake will inevitably introduce additional closed orbit errors in the ring. How these bumps are managed is of great importance.

For the coupled spin resonances it was first necessary to develop the means to better assess their strength and behavior. This was accomplished through improvements to the existing DEPOL algorithm in order to account for coupling. After testing the new DEPOL algorithm during the 2002 polarized proton run we used it to search for a solution to the problem coupled spin resonances. One solution entailed the installation of six skew quadrupoles in the 15th straight section in every other super-period. Using these skew quadrupoles together with the existing skew quadrupole in the 17th straight section our theoretical calculations showed that the remaining coupled spin resonances could be effectively suppressed. This was achieved not through the traditional technique of global or local machine decoupling but rather through a spin matching mechanism. Using skew quadrupoles in this way to suppress

a coupled spin resonance has been demonstrated for first time here.

Given that there is a strong impetus to develop and install a new stronger partial snake in the AGS, questions about how to handle the coupled spin resonance remains. Although a helical snake should minimize coupling, still longitudinal fields will still exist especially since we are working with much higher overall fields. In addition, rolls in the main magnet will ensure that coupled spin resonances will still remain an issue. One possible solution is to push the coupled snake resonances through the spin tune gap as well. This solution still needs a more thorough exploration to determine its feasibility. Another solution is the installation of a family of six skew quadrupoles since it has been shown how to effectively suppress these resonances through their careful use.

The polarization transfer efficiency of RHIC fared much better than the AGS's, due to the successful operation of the two Siberian snakes in each ring. By using measured field data taken from a fixed surface we were able to extrapolate a full field map. A novel technique was employed to enable the OPERA-TOSCA finite element analysis software to generate a full 3D field map. Using these maps we could then establish the operating currents necessary to achieve a spin tune of 1/2. These calculations were tested in a limited way using the ac dipole and the location of the 1/4 snake resonance to determine the bounds of our predictions.

Despite the successful operation of the snakes, the ability of RHIC to achieve a high polarization transfer efficiency varied. Thus it was vital that an understanding of those factors which were critical to polarization be understood. In the process of trying to establish these causes we found for the

first time evidence for the existence of higher snake resonances in RHIC. These snake resonances consisted of an odd order coupled snake resonances at horizontal tune of 3/14 and a even order snake resonances at 1/4. Theoretical calculations had predicted the existence of the coupled snake resonance at 3/14, yet it was not initially anticipated that the level of coupling in RHIC would be so high as to make it an issue. Unlike 3/14 coupled snake resonance, the 1/4 snake resonance was anticipated but its incursion into the operating tune space was greater due to the existence of large closed orbit errors. The behavior of both of these resonances seemed to support the current theory of snake resonances. An estimate of the imperfection resonance strength based on theory was in good agreement with previously calculations.

Future polarized proton runs in RHIC should pay much attention to closed orbit correction so that the impingement of the 1/4 snake resonance can be lessened. Additionally the impact of the 3/14 coupled snake resonance needs to be taken into account. This places a premium on the work of decoupling as well as tune control along the ramp, in order to avoid the effect of the 3/14 coupled snake resonance.

Appendix A

Derivation of Decoupling Matrices

Given a Coupled Matrix,

$$M = \begin{pmatrix} A & B \\ C & D \end{pmatrix}, \tag{A.1}$$

where A, B, C, D and Q are all 2×2 submatrices of sympletic matrix M. There may exists a 4×4 symplectic matrix,

$$R = \frac{1}{\sqrt{1 + |Q|}} \begin{pmatrix} I & \overline{Q} \\ -Q & I \end{pmatrix} \tag{A.2}$$

which can transform M to an uncoupled basis,

$$M = \overline{R} U R. \tag{A.3}$$

Here the over-line indicates a sympletic conjugate defined as $\overline{R} = -SR^TS$ and S is defined as,

$$S = \begin{pmatrix} 0 & 1 & 0 & 0 \\ -1 & 0 & 0 & 0 \\ 0 & 0 & 0 & 1 \\ 0 & 0 & -1 & 0 \end{pmatrix}. \tag{A.4}$$

In this case the simplectic conjugate of R is also its inverse. U is the block diagonal matrix,

$$U = \begin{pmatrix} E & 0 \\ 0 & F \end{pmatrix}. \tag{A.5}$$

From Eq. (A.3) we can see that the elements of M become,

$$\begin{aligned} A = \frac{(E + \overline{Q}FQ)}{1 + |Q|} \quad B = \frac{E\overline{Q} - \overline{Q}F)}{1 + |Q|} \\ C = \frac{(QE - FQ)}{1 + |Q|} \quad D = \frac{(QE\overline{Q} + F)}{1 + |Q|}. \end{aligned} \tag{A.6}$$

If we then add $\overline{A} + A$ and recall that this equals $I\mathrm{tr}A$ we can obtain,

$$\begin{aligned} I\mathrm{tr}A &= \frac{(E + \overline{E} + \overline{Q}FQ + \overline{Q}\,\overline{F}Q)}{1 + |Q|} \\ &= \frac{(I\mathrm{tr}E + \overline{Q}(\mathrm{tr}F)Q)}{1 + |Q|} \\ \\ \mathrm{tr}A &= \frac{(\mathrm{tr}E + |Q|\mathrm{tr}F)}{1 + |Q|}. \end{aligned} \tag{A.7}$$

Likewise we can add $\overline{D} + D$ to obtain,

$$\begin{aligned} I\mathrm{tr}D &= \frac{(F + \overline{F} + Q\overline{E}\,\overline{Q} + QE\overline{Q})}{1 + |Q|} \\ &= \frac{(I\mathrm{tr}F + Q(\mathrm{tr}E)\overline{Q})}{1 + |Q|} \end{aligned}$$

$$\mathrm{tr}D = \frac{(\mathrm{tr}F + |Q|\mathrm{tr}E)}{1 + |Q|}. \tag{A.8}$$

Subtracting Eq. (A.8) from (A.7) yields,

$$\mathrm{tr}(A - D) = \frac{1 - |Q|}{1 + |Q|}\mathrm{tr}(E - F). \tag{A.9}$$

Adding $B + \overline{C}$ we get,

$$B + \overline{C} = \frac{|Q|\mathrm{tr}(E - F)}{1 + |Q|}. \tag{A.10}$$

Combining Eq. (A.9) and (A.10) gives

$$\overline{Q} = \frac{(B + \overline{C})(1 - |Q|)}{Tr(A - D)}. \tag{A.11}$$

Multiplying both sides by the simplectic conjugate we can solve for $|Q|$,

$$\begin{aligned} |Q| &= \frac{|B + \overline{C}|(1 - |Q|)^2}{(\mathrm{tr}(A - D))^2} \\ |Q| &= 1 + \frac{\mathrm{tr}(A - D)\left(\frac{\mathrm{tr}(A-D)}{2} \pm \sqrt{\frac{(\mathrm{tr}(A-D))^2}{4} + |B + \overline{C}|}\right)}{|B + \overline{C}|}. \end{aligned} \tag{A.12}$$

Substituting back into Eq. (A.11) finally gives Q in terms of the elements of the uncoupled matrix,

$$\overline{Q} = -\left(\frac{\mathrm{tr}(A-D)}{2} \pm \sqrt{|B+\overline{C}| + \frac{(\mathrm{tr}(A-D))^2}{4}}\right)\frac{B+\overline{C}}{|B+\overline{C}|}. \qquad \text{(A.13)}$$

Appendix B

Method of Phase Factoring

If we consider the elements in Eq. (3.16) and (3.17) we can see that a common piece takes on the following form,

$$\frac{(z_2' - iK\rho z_2)e^{iK\theta_2} - (z_1' - iK\rho z_1)e^{iK\theta_1}}{k_z - (K\rho)^2}. \tag{B.1}$$

Expanding each factor we find,

$$z_1 e^{iK\theta_1} = e^{iK\theta_1}\left[R_{3,1}u_1 + R_{3,2}u_1' + R_{3,3}v_1 + R_{3,4}v_1'\right], \tag{B.2}$$

$$\begin{aligned} e^{iK\theta_1}u_1 &= \sqrt{\beta_u[L]\epsilon_u}\cos\left[-(\mu_u[L] + \mu_u[L_{max}]n)2\pi\right]e^{iK\theta_1} \\ &= \frac{\sqrt{\beta_u[L]\epsilon_u}}{2}\left(\exp(-i2\pi\mu_u[L])e^{-i(2\pi\mu_u[L_{max}]n - K\theta_1)}\right. \\ &\left. + \exp(i2\pi\mu_u[L])e^{i(2\pi\mu_u[L_{max}]n + K\theta_1)}\right), \end{aligned} \tag{B.3}$$

$$
\begin{aligned}
e^{iK\theta_1}u_1' = & \sqrt{\frac{\epsilon_u}{\beta_u[L]}}\,[-\alpha_u[L]\cos\left[-(\mu_u[L]+\mu_u[L_{max}]n)2\pi\right]+ \\
& \sin\left[-(\mu_u[L]+\mu_u[L_{max}]n)2\pi\right]]\,e^{iK\theta_1} \\
= & \sqrt{\frac{\epsilon_u}{\beta_u[L]}}\left(-(\alpha_u[L]+i)\exp(-i2\pi\mu_u[L])e^{-i(2\pi\mu_u[L_{max}]n-K\theta_1)}\right. \\
& \left.-(\alpha_u[L]-i)\exp(i2\pi\mu_u[L])e^{i(2\pi\mu_u[L_{max}]n+K\theta_1)}\right). \qquad \text{(B.4)}
\end{aligned}
$$

Here L indicates the lattice indexed position, L_{max} the final index and n the index indicating the number of passes through the lattice. $R_{i,j}$ are the elements of the decoupling R matrix and u , v are the coordinates in the uncoupled basis. The $e^{iK\theta_1}v_1$ and $e^{iK\theta_1}v_1'$ terms have the same form as Eqs. (B.3) and (B.4) replacing u with v. Clearly all the terms in Eq. (B.1), when summed over the lattice N number of times can have the following four terms factored out,

$$
\begin{aligned}
E_u(N)_\pm &= \sum_{n=0}^{N} e^{i2\pi n(K\pm\mu_u[L_{max}])} \\
&= \pm e^{iN\pi(K\pm\mu_u[L_{max}])}\frac{\sin\left(\pi(N+1)(K\pm\mu_u[L_{max}])\right)}{\sin\left(\pi(K\pm\mu_u[L_{max}])\right)} \\
E_v(N)_\pm &= \sum_{n=0}^{N} e^{i2\pi n(K\pm\mu_v[L_{max}])} \\
&= \pm e^{iN\pi(K\pm\mu_v[L_{max}])}\frac{\sin\left(\pi(N+1)(K\pm\mu_v[L_{max}])\right)}{\sin\left(\pi(K\pm\mu_v[L_{max}])\right)} \qquad \text{(B.5)}
\end{aligned}
$$

Since $\mu_v[L_{max}] = \nu_v$ and $\mu_u[L_{max}] = \nu_u$ Eq.(B.5) reduces to Eq.(3.19). Thus a sum over N passes of the lattice can be reduced to a sum just over L if the appropriate terms are multiplied by their enhancement factor.

Appendix C

Transformation of Emittances to Coupled Basis

In General we can define a sigma matrix as the variance of the beam's distribution:

$$\sigma_{xz} = \begin{pmatrix} < x^2 > & < xx' > & < xz > & < xz' > \\ < x'x > & < x'^2 > & < x'z > & < x'z' > \\ < zx > & < zx' > & < z^2 > & < zz' > \\ < z'x > & < z'x' > & < z'z > & < z'^2 > \end{pmatrix}. \tag{C.1}$$

In the uncoupled u and v basis we can the sigma matrix in terms of its Twiss parameters:

$$\sigma_{u-v} = \begin{pmatrix} \epsilon_u\beta_u & -\epsilon_u\alpha_u & 0 & 0 \\ -\epsilon_u\alpha_u & \epsilon_u\gamma_u & 0 & 0 \\ 0 & 0 & \epsilon_v\beta_v & -\epsilon_v\alpha_v \\ 0 & 0 & -\epsilon_v\alpha_v & \epsilon_v\gamma_v \end{pmatrix}. \tag{C.2}$$

If we transform this to the coupled x-z basis, then

$$\sigma_{xz} = R\sigma_{u-v}\overline{R}. \tag{C.3}$$

We can obtain expressions for $< x^2 >$ and $< z^2 >$ in terms of the Twiss parameters in the uncoupled basis and the rotation matrix elements:

$$\begin{aligned} < x^2 >= \epsilon_u \left[\overline{R}_{1,1}R_{1,1}\beta_u - \overline{R}_{1,1}R_{1,2}\alpha_u - \overline{R}_{2,1}R_{1,1}\beta_u + \overline{R}_{2,1}R_{1,2}\gamma_u\right] \\ +\epsilon_v \left[\overline{R}_{3,1}R_{1,3}\beta_v - \overline{R}_{3,1}R_{1,4}\alpha_v - \overline{R}_{4,1}R_{1,3}\alpha_v + \overline{R}_{4,1}R_{1,4}\gamma_v\right], \end{aligned} \tag{C.4}$$

$$\begin{aligned} < z^2 >= \epsilon_u \left[\overline{R}_{1,3}R_{3,1}\beta_u - \overline{R}_{1,3}R_{3,2}\alpha_u - \overline{R}_{2,3}R_{3,1}\beta_u + \overline{R}_{2,3}R_{3,2}\gamma_u\right] \\ +\epsilon_v \left[\overline{R}_{3,3}R_{3,3}\beta_v - \overline{R}_{3,3}R_{3,4}\alpha_v - \overline{R}_{4,3}R_{3,3}\alpha_v + \overline{R}_{4,3}R_{3,4}\gamma_v\right]. \end{aligned} \tag{C.5}$$

Since $< x^2 >= \sigma_x$ and $< z^2 >= \sigma_z$ are what the profile detectors measures it is easy to solve for ϵ_u and ϵ_v.

Bibliography

[1] E.D. Courant and R.D. Ruth, *The Acceleration of Polarized Protons in Circular Accelerators*, BNL 51270 1980.

[2] A.Lehrach et al.,Suppressing intrinsic spin harmonics at the AGS, C-A/AP#11 (2000).

[3] Ya.S. Derbenev and A.M. Kondratenko, Zh. Eksp. Teor. Fiz. 62, 430 (1972) [Sov. Phys. JETP 35, 230 (1972)]; Ya.S. Derbenev et. al., Part. Accel. 8, 115 (1978).

[4] A.D.Krish et al., Phys. Rev. Lett. **63**, 1137 (1989)

[5] W.W.MacKay et al. *Commissioning and future Plans for polarized protons in RHIC* Proc. of PAC01, Chicago, 24.

[6] T.Roser et al. *Accelerating and colliding polarized protons in RHIC with Siberian Snakes* Proc. of EPAC02, Paris, 209.

[7] S.Y.Lee and S. Tepikian, Phys. Rev. Lett. **56**, 1635 (1986); S. Tepikian, Ph.D. thesis, State University of New York at Stony Brook, 1986 (unpublished)

[8] S.Y.Lee, (1992) Phys.Rev.E **47**, N5.

[9] M. Froissart, and R.Stora, *Nucl. Inst. Meth.* **7**, 297 (1960)

[10] L.C. Teng, Concerning n-Dimensional Coupled Motion. **FN** 229, FNAL, (1971).

[11] H.Grote and F.C.Iselin *Methodical Accelerator Design Program Version 8.23* CERN/SL/90-13(AP).

[12] A. Zelenski, et al., *Proceedings of the 9th International Conference on Ion Sources*, Rev. Sci.Inst., Vol. **73** , No.2, p.888(2002)

[13] H.Huang et al., Phys. Rev. Lett. **73**, 2982 (1994).

[14] M.Bai et al, Phys. Rev **E56**, 6002 (1997).

[15] H.Spinka et al., Nucl. Instrum. Methods 211, 239 (1983).

[16] H.Huang personal communication.

[17] H. Huang, Ph. D Thesis, Indiana University (1995)

[18] Chart obtained from Kevin Brown.

[19] C.J.Gardner, et.al *Observation and Measurement of Linear Coupling in the AGS* AGS Studies Report, N224, 1987

[20] F.Pilat, et.al *Coupling measurement and correction during RHIC run 2001 and development for 2003*, C-A/AP 77, July 2002

[21] T.Roser, *Proc.Workshop on Siberian Snakes and Depolarizing Techniques* (1989) p.144.

[22] S.Y.Lee ,Spin Dynamics and Snakes in Synchrotrons, World Scientific p. 25-42, 93, 1997

[23] H.Huang et al, *Overcomming an Intrinsic Depolarizing Resonance with a Partial Snake at the Brookhaven AGS*, (2002) to be published.

[24] I.Alekseev, et. al *Design Manual Polarized Proton Collider at RHIC* July 1998, pages 35-48

[25] E.D. Courant, *Orbit Matrices for Helical Snakes* AGS/RHIC/Spin Note, BNL No. 4 (1996)

[26] E.D. Courant, *Hybrid Helical Snakes and Rotators for RHIC*, AGS/RHIC/Spin Note, BNL No. 10 (1996)

[27] M.J.Syphers, *Closed Orbit Errors from Helical Dipole Magnets*, AGS/RHIC/Spin Note, BNL No. 16 (1996)

[28] K.Hatanaka, T.Katayama,T.Tominaka, *Maxwellian Field Expansion of Helical Magnet*, IEEE 3416 (1998).

[29] W.Fischer, M. Okamura, *Parameterization and measurements of Helical Magnetic Fields*, IEEE 3341 (1998).

[30] TOSCA and OPERA commercial software version 8.0.

[31] A.U.Luccio, *Trends in Collider Spin Physics* pp 244 World Scientific (1997)

[32] V.Ranjbar et al., *Mapping out the full spin resonance structure of RHIC* Proc. of PAC01, Chicago, 3177.

[33] M.Bai, et.al *RHIC Spin Flipper Commissioning* Proc. of EPAC02, Paris, 299.

[34] A.U.Luccio, *Field Map Generated Matrices for Spin Tracking*, RIKEN-AF-NP-235 (1996)

[35] Chart obtained from Alfredo Luccio.